DIPLOMARBEIT

Titel der Diplomarbeit

„The clathrates $Ba_8TM_xGe_{46-x-y}\square_y$ and $Ba_8TM_xSi_{46-x}$ (TM = Ag, Au): phase equilibria and physical properties"

Verfasserin

Isolde Zeiringer

angestrebter akademischer Grad

Magistra der Naturwissenschaften (Mag. rer. nat.)

Wien, 2010

Studienkennzahl lt. Studienblatt:	A 419
Studienrichtung lt. Studienblatt:	Chemie
Betreuerin / Betreuer:	Univ. Prof. Dr. Peter Franz Rogl

Table of Contents

Abstract

In the present diploma thesis, 4 ternary systems containing clathrate type-I compounds with

K_4Ge_{23-x} structure type were studied to elucidate the homogeneity region of the clathrates, to establish phase relations around the clathrate phase and to prepare single-phase clathrate samples for thermoelectric properties measurements.

In the Ba – Ag – Ge system the clathrate I solid solution ranges at 800°C from binary $Ba_8Ge_{43}\square_3$ ($\square$ is a vacancy) to $Ba_8Ag_{5.3}Ge_{40.7}$. Besides $Ba_8Ag_xGe_{46-x-y}\square_y$ another clathrate type exists in this system. Clathrate type-IX (Ba_6Ge_{25} structure type) has a maximum solubility of 1.5 at% silver at 800°C. Two ternary compounds that were already reported have been confirmed at 800°C. but in this work the homogeneity region has been established. $BaAg_{2-x}Ge_{2+x}$ ($ThCr_2Si_2$ structure type) has a quite large homogeneity region extending from $BaAg_{1.3}Ge_{2.7}$ to $BaAg_{1.8}Ge_{2.2}$. For the second ternary compound the homogeneity range is limited to only a few atomic percent of silver (from $BaAg_{0.5}Ge_{1.5}$ to $BaAg_{0.7}Ge_{1.3}$).

As the binary $Ba_8Ge_{43}\square_3$ clathrate I compound exists only between 770 and 810°C samples annealed at 600°C were investigated to find the stability range of the clathrate $Ba_8Ag_xGe_{46-x-y}\square_y$ at 600°C: the homogeneity region is limited and extends from about 6.6 to 9.8 at% silver. The solubility range for the other two ternary compounds is only slightly different with respect to 800°C. $BaAg_5$ (solves about 4at% germanium) is observed as a new phase at 600°C.

The Ba – Au – Ge system contains also a large solubility range for the ternary clathrate I $Ba_8Au_xGe_{46-x-y}\square_y$. Starting from the binary $Ba_8Ge_{43}\square_3$ the maximum solubility for gold at 800°C was about 12 at%. Clathrate type-IX exhibits a solubility limit of 2.7 at% gold at this temperature. At about 20 at% barium the ternary phase $Ba(AuGe)_4$ ($BaNiSn_3$ structure type within the germanium rich part) can be found. With higher gold content, the powder patterns indicate a different structure type and the phase extends up to about 60 at% gold. The second ternary phase found in this system is $Ba(AuGe)_2$ with AlB_2 structure type. It shows a quite large solubility range from $BaAu_{0.5}Ge_{1.5}$ to $BaAu_{0.9}Ge_{1.1}$ at 800°C. A third ternary phase with about 60 at% gold, 12 at% barium and 28 at% germanium exists in the gold rich part of the isothermal section.

The other two ternary systems studied are Ba – Ag – Si and Ba – Au – Si. As the binary barium – silicon phase diagram does not contain a clathrate compound silver and gold are observed to stabilize a ternary clathrate of type I in a limited homogeneity region at 800°C.

In the Ba – Ag – Si system it extends from $Ba_8Ag_{4.3}Si_{41.7}$ to $Ba_8Ag_{5.4}Si_{40.6}$. Two ternary compounds are reported in this system. At 800°C $Ba_4Ag_2Si_6$ ($Ba_4Li_2Si_6$ structure type) does not show a

homogeneity range and the part of the isothermal section with the second ternary phase $Ba_{32}Ag_{20}Si_{30}$ has not been investigated.

The homogeneity range of the ternary clathrate I $Ba_8Au_xSi_{46-x}$ was found to be larger than for the $Ba_8Ag_xSi_{46-x}$ clathrates and extends from about 7.4 to 11.6 at% gold. Also in the Ba – Au – Si system $Ba(AuSi)_2$ with AlB_2 structure type can be found with a large homogeneity region. It ranges from $BaAu_{0.4}Si_{1.6}$ to stoichiometric $BaAuSi$. The binary phase $BaAu_2$ (AlB_2 structure type) solves about 7.5 at% silicon at 800°C. Further investigations will be necessary for the gold rich part of the isothermal section. At about 20 at% barium a $Ba(AuSi)_4$ phase was observed and another gold rich phase with about 12at% barium.

In addition to the investigations concerning the isothermal sections at 800°C, several clathrate samples were prepared with "ball-milling" and "hot-pressing" to measure thermoelectric properties. For the 3 samples $Ba_8Ag_5Si_{41}$, $Ba_8Au_{5.1}Si_{40.9}$ and $Ba_8Au_6Si_{40}$ electrical resistivity and thermopower were measured in the temperature range between 4.2 and about 900 K and thermal conductivity was measured between 6K and room temperature.

Kurzfassung

In der vorliegenden Diplomarbeit wurden 4 ternäre Systeme untersucht, die ternäre Clathrate mit K_4Ge_{23-x} Strukturtyp der Zusammensetzung $Ba_8TM_xGe_{46-x-y}\square_y$ und $Ba_8TM_xSi_{46-x}$ (TM = Ag, Au; $\square$ ist eine Leerstelle) beinhalten, um deren Homogenitätsbereiche und die Phasenverhältnisse um die Clathrat Phase zu bestimmen. Weiters wurden aus den Erkenntnissen einphasige Proben hergestellt um die thermoelektrischen Eigenschaften zu messen.

Im Ba – Ag – Ge System reicht bei 800°C der Homogenitätsbereich der Clathrate I Phase vom binären $Ba_8Ge_{43}\square_3$ bis zu $Ba_8Ag_{5..3}Ge_{40.7}$. Außerdem findet man neben Clathrate Typ-I auch den Typ-IX (Ba_6Ge_{25} Strukturtyp) mit einer maximalen Silberlöslichkeit bei 800°C von 1.5at%. Des weiteren werden bei 800°C zwei bereits in der Literatur beschriebene ternäre Verbindungen beobachtet. $BaAg_{2-x}Ge_{2+x}$ ($ThCr_2Si_2$ Strukturtyp) hat einen ziemlich großen Homogenitätsbereich von $BaAg_{1..3}Ge_{2.7}$ bis $BaAg_{1.8}Ge_{2.2}$. Auch für die 2. ternäre Phase konnte bei 800°C ein kleiner Homogenitätsbereich beobachtet werden (von $BaAg_{0..5}Ge_{1..5}$ bis $BaAg_{0.7}Ge_{1.3}$).

Da im binären Phasendiagramm Barium - Germanium $Ba_8Ge_{43}\square_3$ nur zwischen 770 und 810°C vorhanden ist, wurden die Phasenverhältnisse auch bei 600°C untersucht. Der Homogenitätsbereich der Clathrate I Phase erstreckt sich bei 600°C nur mehr von ~ 6.6 bis 9.8 at% Silber wohingegen für die anderen beiden ternären Verbindungen nur geringfügige Unterschiede zu beobachten sind. Als neue Phase tritt bei 600°C $BaAg_5$ auf mit einer maximalen Löslichkeit von 4at% Germanium.

Auch das System Ba – Au – Ge zeigt bei 800°C einen weitreichenden Homogenitätsbereich von der binären Verbindung $Ba_8Ge_{43}\square_3$ bis hin zu $Ba_8Au_{6.3}Ge_{39.7.}$ Clathrate Typ-IX mit einer maximalen Löslichkeit von 2.7 at% Gold wird auch in diesem System bei 800°C gefunden. Bei ~ 20 at% Barium wird die ternäre Phase $Ba(AuGe)_4$ beobachtet ($BaNiSn_3$ Strukturtyp). Mit zunehmendem Goldgehalt der Probe, ändert sich der Strukturtyp der Phase und die Phase endet bei ungefähr 60 at% Gold. Die zweite ternäre Phase, die beobachtet werden konnte, ist $Ba(AuGe)_2$ mit AlB_2 Strukturtyp. Sie zeigt einen ziemlich großen Homogenitätsbereich von $BaAu_{0.5}Ge_{1.5}$ bis $BaAu_{0.9}Ge_{1.1}$ bei 800°C. Eine dritte ternäre Phase wird im Gold-reichen Teil des isothermen Schnittes bei ~ 60 at% Gold, 12 at% Barium und 28 at% Germanium beobachtet.

In den beiden anderen untersuchten ternären Systeme Ba – Ag – Si und Ba – Au – Si existiert im binären Barium – Silizium Phasendigramm keine Clathrat Typ-I Verbindung. Die Homogenitätsbereiche sind daher limitiert für diese Systeme.

Im Ba – Ag – Si System erstreckt sich dieser Bereich nur von $Ba_8Ag_{4.3}Si_{41.7}$ bis $Ba_8Ag_{5.4}Si_{40.6}$ bei 800°C. Zwei weitere ternäre Verbindungen sind in diesem System bekannt. Dies sind zum einen $Ba_4Ag_2Si_6$ ($Ba_4Li_2Si_6$ Strukturtyp) und $Ba_{32}Ag_{20}Si_{30}$ (dieser Teil des isothermen Schnittes wurde nicht untersucht).

Der Homogenitätsbereich für Typ-I Clathtrate $Ba_8Au_xSi_{46-x}$ ist bei 800°C größer als für

die Silber-Silizium Clathrate und erstreckt sich von ~7.4 bis 11.6 at% Gold. Die ternäre Phase $Ba(AuSi)_2$ (AlB_2 Strukturtyp) zeigt bei 800°C auch im System Ba – Au – Si einen großen Homogenitätsbereich von $BaAu_{0.4}Si_{1.6}$ bis zur stöchiometrischen Verbindung BaAuSi. Die binäre Verbindung $BaAu_2$ (AlB_2 Strukturtyp) löst bei 800°C ~7.5 at% Silizium. Zwei weitere goldreiche Phasen wurden im Bereich um ~ 20at% Barium und ~12 at% Barium gefunden.

Zusätzlich zu den Phasendiagrammen wurden Proben durch Vermahlen in der Kugelmühle und anschließendem Heißpressen hergestellt um die thermoelektrischen Eigenschaften an dichten Proben messen zu können. Von den 3 Proben $Ba_8Ag_5Si_{41}$, $Ba_8Au_{5.1}Si_{40.9}$ und $Ba_8Au_6Si_{40}$ wurden der elektrische Widerstand und der Seebeck-Koeffizient zwischen 4.2 und 900 K gemessen und die Wärmeleitfähigkeit zwischen 6 K und Raumtemperatur.

Introduction

The best known representatives of the clathrate family are crystal hydrates of gases and liquids. The first one, which was discovered by Davy in 1811, was chlorine hydrate, but its crystal structure was primary established in 1952 by Allen. In the 1960's the first silicates [1] and silicides [2] later also germanides and stannides [3] which are isostructural to gas hydrates were characterised. Since clathrates were found to be promising thermoelectric materials [4,5,6] and superconductivity was discovered in Na and Ba doped silicon clathrates [7], clathrates have been studied intensively and lots of new types of them were synthesised (type I, II, III, VIII, IX)[8]. Several type-I clathrates with the composition $Ba_8TM_xGe_{46-x}$ or $Ba_8TM_xSi_{46-x}$ (TM = Cu, Ag, Au, Ni, Pt, Pd) have been reported by Cordier and Woll [9]. They belong to the clathrates with the general formula $M_x(Si,Ge)_{46}$ (M = alkali or alkaline-earth) and the primitive centrosymmetrical cubic space group P m-3n. In this structure, the Si or Ge framework atoms can be substituted by transition metals like Ni, Pd, Pt, Cu, Ag, Au [9]. This 46 framework atoms occupy 3 different sites: 6d, 16i and 24k. The three dimensional framework contains large cavities which are polyhedra with pentagonal and hexagonal faces [8]. Two different types of polyhedra can be found in clathrate type-I structures. The first one is the pentagonal dodecahedron. It contains 12 pentagonal faces $[5^{12}]$ and the second one is the larger tetrakaidecahedron containing 12 pentagonal and 2 hexagonal faces $[5^{12}6^2]$.
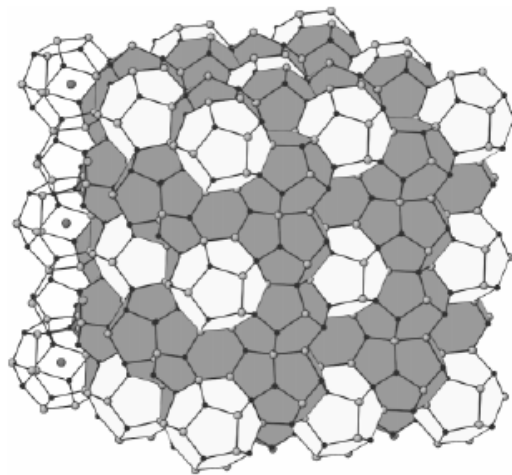

Fig.1: polyhedral representation of the type-I clathrates structure [8]

The alkali or alkaline - earth atoms can be found inside this cavities and each unit cell contains two small and 6 large of them (2a and 6c site).

In the first part of this work investigations concerning the clathrate I solid solutions and the partial isothermal sections at 800°C for the 4 ternary systems Ba – Ag - Ge, Ba – Ag - Si, Ba – Au - Ge and Ba – Au - Si were done.

The second part contains the preparation of the clathrates with nominal composition $Ba_8Ag_5Si_{41}$,

$Ba_8Au_5Si_{41}$ and $Ba_8Au_6Ge_{40}$ by ball milling and hot pressing and their physical properties (thermopower, resistivity and thermal conductivity).

References

[1] B. Kamb S*cience* **148** 232 (1965)

[2] J.S. Kasper, P. Hagenmuller, M. Pouchard *Science* **150** 1713 (1965)

[3] Yu N Grin, L.Z. Melekhov, K.A: Chutonov, S.P. Yatsenko *Kristallograviya* **32** 497 (1987)

[4] G.A. Slack, "New Materials and Performance Limits for Thermoelectric Cooling," CRC Handbook of Thermoelectrics, CRC Press (Boca Ratan, 1995), 407 - 440

[5] G.A. Slack, "Design Concept for Improved Thermoelectric Materials," *Mat. Res. Soc. Symp. Proc.*, **478** (1997) 47-54

[6] G.S. Nolas, J. L. Cohn, G. A. Slack, and **S.** B. Schujman, "Semiconducting Ge Clathrates: Promising Candidates for Thermoelectric Applications," *Appl. Phys. Lett*. **73**, No. 2 (1998) 178-180.

[7] H. Kawai, H. O. Horie, S. Yamanaka and M. Ishikawa, *Phys.Rev.Lett.* **74**, 1427 (1995) S.Yamanaka, E. Enishi, H. Fukuoka and M. Yasukawa, *Inorg. Cem*. **39**, 56 (2000)

[8] K.A. Kovnir, A.V. Shevelkov *Russian Chemical Review* **73** 923 – 938 (2004)

[9] G Cordier, P Woll *J. Less-Common. Met.* **169** (1991) 291

The System Ag – Ba – Ge

INTRODUCTION

Although several investigations dealt with compounds from the Ag – Ba - Ge system, there is still little known about phase equilibria in the ternary system and about the solubility range of ternary phases at a defined temperature. Besides the type-I clathrate, $Ba_8Ag_6Ge_{40}$, for which full atom order has been elucidated from an X-ray single crystal study [1] and for which thermoelectric properties have been described (p-type material) [2], two other ternary compounds have been reported in literature (a) $BaAg_{0.8}Ge_{1.2}$ with the AlB_2 structure type and a small undefined homogeneity region at 550°C [3] and (b) $BaAg_2Ge_2$ with the $ThCr_2Si_2$ structure type [4].

The aim of the present research is three-fold: (a) to provide consistent information on the phase relations in isothermal sections at 800 and 600°C for the region with Ba-contents less than 33 at.%, (b) to provide details on the homogeneity regions of binary and ternary compounds in combination with atom order in the corresponding crystal structures, and (c) to provide thermoelectric data on the clathrate type I as a function of temperature and of composition throughout its homogeneity region.

EXPERIMANTAL DETAILS

Samples (~1g) for the isothermal section were prepared by arc melting from the pure elements (Ba 99.9, Ag 99.9 and Ge 99.999 mass%) under an argon atmosphere. The weight loss was in all cases lower then 1 mass%. The arc-melted buttons were vacuum-sealed in quartz tubes and annealed at 800°C for 1 week, characterized and subdued to another annealing at 600°C for 1 month.

For the characterisation of the samples, X-ray powder diffraction (XRPD), electron probe microanalysis (EPMA) and differential thermal analysis (DTA) were used. X-ray powder diffraction was performed on a Guinier-Huber image plate recording system (monochromatized $CuK\alpha_1$ radiation) and lattice parameters were calculated by least-square fits using Ge or Si as internal standard (a_{Ge} = 0.565791 and a_{Si} = 0.543106 nm). Rietveld refinements were made with the FULLPROF program [5]. To image the micro - structure of the samples a Philips XL 30 ESEM-FEG (emission environmental scanning electron microscope) was used and the chemical composition was determined from electron probe microanalysis (EDX detector) using a Buehler Simplimett 3 and a JSM 6400 SEM equipment. Differential thermal analysis was carried out in a STA 409 Netsch differential scanning calorimeter with a heating rate of 10 K/min (5, 1, 0.1 K/min) in Y_2O_3 protective coated Al_2O_3 crucibles under a stream of argon (6N, 70 ml/min).

 Four samples (of about 1 cm³ each) with nominal composition $Ba_8Ag_xGe_{46-x-y}\square_y$ (x = 2,3,4,5) ($\square$ … vacancy) were prepared in a different way in order to reach a relative density (ρ/ρ_X) higher than 96% for physical properties measurements (thermopower, resistivity and thermal conductivity). For each sample, 5 alloys of 1-2g were prepared by argon arc melting from the pure elements. After arc-melting they were sealed under vacuum into quartz tubes, remelted at 900°C for ~2 hours, and finally annealed for 5 days at 800°C. Powders - obtained from these alloys via ball milling in a Vario Planetenmühle (Pulverisette 4) - were then compacted in a hot press (HP W 200/250-2200-200-Ks, FCT System GmbH) at 700°C and a pressure of 4 kN under an argon atmosphere followed by another annealing in sealed quartz tubes at 800°C for 5 days.

RESULTS AND DISCUSSION

The clathrate I solid solution $Ba_8Ag_xGe_{46-x-y}\square$

The solubility range of the ternary type-I clathrate was studied by XRPD and EPMA on a series of samples with nominal composition $Ba_8Ag_xGe_{46-x}$ (x = 1,2,3,4,5,6,8). Table 1 shows a comparison of the EPMA data with the results of Rietveld refinement of the X-ray spectra. In all cases the spectra could be fully indexed in the basis of a cubic clathrate type I lattice with minor amounts of Ge (< 2.2%). Starting from the binary $Ba_8Ge_{43}\square_3$ the maximal solubility at 800°C for silver was found to be 5.3 atoms per formula unit (9.8 at%) with EPMA (dashed line in Fig. 1). The lattice parameters show a linear increase with increasing silver content up to 4.8 silver atoms per unit cell (a = 1.0840(9) nm). Samples with higher silver content show only slightly different lattice parameters and are close to that reported by Cordier and Woll for a single crystal of stoichiometric $Ba_8Ag_6Ge_{40}$ (melted at 1300°C and cooled at 100K/hr; a = 1.0840(1) nm) [1].

Table 1 shows a comparison of the EPMA data with the results of Rietveld refinement of the X-ray spectra. The decreasing Ba-content with increasing silver is related to the amount of vacancies in the crystal lattice $Ba_8Ag_x\square_yGe_{46-x-y}$. Assuming fully occupied Ba sites in the clathrate lattice (sites 2a and 6c in space group Pm3n; standardized with structure tidy), the vacancy concentrations calculated from EPMA, disagree only slightly with the amount of vacancies obtained from Rietveld refinement. The amount of vacancies does not decrease linearly with the increasing silver content but all voids vanished at a composition of 4.8 atoms of silver per unit cell (Fig. 2). In addition to the experimental data, there are two boundary models drawn in figure 3. Model A assumes, that there is only a substitution of germanium atoms and no filling of vacancies $Ba_8Ag_x\square_3Ge_{43-x}$. The second model delineates first all the vacancies and after that the Ge / Ag exchange occurs. The experimental data are in between these two models. This means that filling vacancies and

substitution of Ge atoms takes place simultaneously. This is in quite good agreement with the results reported for other ternary clathrates [Ba-Zn-Ge [6], Ba-Pt-Ge [7], BaPdGe [9], BaCdGe [10]…].

Figure 3 shows the XRPD pattern of samples with increasing silver content and the Rietveld refinement for one of them. No extra reflections for a larger unit cell a' = 2a as reported [11] for the binary $Ba_8Ge_{43}\square_3$ were observed. The refinement in all cases confirmed the Ba atoms in the sites 2a (0, 0, 0) and 6c $(\frac{1}{4},0,\frac{1}{2})$, Ge atoms in the sites 16i (x, x, x) and 24k (0, y, z), whereas Ag, Ge atoms and vacancies can be found in the 6d $(\frac{1}{4},\frac{1}{2},0)$.(Check if 6c, 6d is from standardized structure) Because refinement of occupancies for three species in one site is not reliable, the Ag content was fixed from EPMA measurements. Cordier et al. [1] as well as Johnsen et al. [2] reported that Ag mostly occupies the 6c site. The refinement for the samples with highest silver content (5.3 silver atoms per formula unit) showed, that a small amount of silver also enters the 24k site in agreement with the findings of Johnsen et al. [2]. In the x-ray powder spectra the increasing silver content can be seen in the intensity ratio of 3 peaks indexed as (222), (320) and (321). The positional parameters y and z of the 24k site, received from Rietveld refinement, decrease with increasing silver content (Fig. 4).

Phase relations at 800°C and at 600°C

The experimental results from Rietveld refinement and EPMA are combined in table 2 and figure 6 and are the basis for the phase triangulation in the isothermal sections at 800°C and 600°C. Type-I clathrate is in equilibrium with clathrate type-IX (Ba_6Ge_{25} structure type). The maximum solubility of silver in clathrate IX at 800°C is 1.5 at% (a = 1.4561(7) nm). Alloys containing moisture sensitive $BaGe_2$ ($BaSi_2$ structure type), quickly decompose on air. For some phases it was not possible to calculate lattice parameter because the XRPD peaks were too weak. At the solubility limit of silver, clathrate I forms a two-phase equilibrium with $BaAg_{2-x}Ge_{2+x}$ ($ThCr_2Si_2$ structure type). At 800°C EPMA data indicate a quite large homogeneity region of about 10 at% for this phase ranging from $BaAg_{1.3}Ge_{2.7}$ (x= 0.7, a = 0.4652(9), c = 1.0606(2) nm) to $BaAg_{1.8}Ge_{2.2}$ (x=0.2, a = 0.4610(7), c = 1.0697(9) nm). The lattice parameter dependency for the homogeneity region is shown in figure 7 ($\frac{c}{a} \sim 2.3$ in all cases). It seems that the homogeneity region does not include the stoichiometric composition at full atom order in contrast to an earlier report by Eisenmann et al. [Eisenmann] on the existence of $BaAg_2Ge_2$ for which single crystals were obtained from an alloys reacted at 1250°C (no further details were given). The Rietveld refinement for a sample in the Ge-rich part of the homogeneity region of $BaAg_{2-x}Ge_{2+x}$ is shown in Fig.8. It confirms the $ThCr_2Si_2$ structure type with a random substitution of silver atoms with germanium atoms in the 4d site of space group I4/mmm (z_{4e}=0.381(9)). The second phase in the refinement is $Ba(Ag_{1-x}Ge_x)_2$ with AlB_2 structure type. Merlo et al. [3] indicated a solid solubility range for $Ba(Ag_{1-x}Ge_x)_2$ at 550°C

(no details were presented). But at 800°C only a quite small homogeneity region can be found between $BaAg_{0.5}Ge_{1.5}$ (x = 0.75; a = 0.4427(1), c = 0.4882(8) nm) and $BaAg_{0.7}Ge_{1.3}$ (x = 0.65; a = 0.4485(1), c = 0.4814(3) nm). The lattice parameter for $BaAg_{0.4}Ge_{1.6}$ comes from an "as-cast" sample (fig. 8) ($\frac{c}{a} \sim$ 1.1 in all cases). EPMA measurements were only made for the sample $BaAg_{0.8}Ge_{1.2}$. The other two values are the nominal composition. The lattice parameter determined by Merlo, are also plotted. The Rietveld refinement for a sample containing $Ba(Ag_{1-x}Ge_x)_2$ as the main phase is shown in figure 9. The two other phases are $BaGe_2$ and $BaAg_{2-x}Ge_{2+x}$ (< 10%).

In the binary barium – germanium system Ba_8Ge_{43} only exists between 770 and 810°C [11]. To find the stability range of clathrate I $Ba_8Ag_xGe_{46-x}$, the partial isothermal section at 600°C was also investigated (fig. 10). At 600°C the homogeneity region of clathrate I is limited. It only extends from about ~ 6.6 to ~ 9.8 at% silver (3.4 ≤ x ≤ 5.3). The results from EPMA measurements and X-ray phase analysis are summed in table 2. The solubility range for $BaAg_{2-x}Ge_{2+x}$ and $Ba(Ag_{1-x}Ge_x)_2$ is only slightly smaller than at 800°C (from 1.45 to 1.7 silver atoms per unit cell for $BaAg_{2-x}Ge_{2+x}$; 0.55≤x≤0.3). Further investigations into the silver rich part will be necessary to find the solubility limit for the $Ba(Ag_{1-x}Ge_x)_2$ phase. As a new phase $BaAg_5$ can be found at 600°C because this part of the phase diagram is in liquid state at 800°C. $BaAg_5$ solves about 4 at% silver at this temperature.

For DTA measurements, samples annealed at 600°C for 1 month were used. The DSC signal for a hot pressed sample (annealed at 800°C) containing clathrate I (4.8 Ag atoms per formula unit) and small amounts of Ge is shown in figure 12. The solidus temperature is about 812°C and the liquidus temperature is 856 °C. The received reaction temperatures from all measured samples are summarised in table 3.

References

[1] G Cordier, P Woll J. Less-Common. Met. 169 (1991) 291

[2] S. Johnsen, B. Thomsen, M. Christensen, G.K.H. Madsen, M. Nygren, B. Inversen
(2007) ICT

[3] F. Merlo, M.L. Fornasini *Journal of Alloys and Compounds* **232,** 289 (1996)

[4] B. Eisenmann, N. May, W. Müller, H. Schäfer, A.Weiss, J. Winter, G. Ziegleder *Z. Naturf. B* **25**
(1970) 1350

[5] J. Rodriguez-Carvajal, FULLPROF, Abstract of the satellite meeting on powder
diffraction of the 15 congress, Int. Union of Crystallography, Talence, 127 (1990)

[6] N. Melnychenko-Koblyuk, A. Grytsiv, L. Fornasari, H. Kaldarar, H. Michor, F.
Röhrbacher, M. Koza. E. Royanian, E. Bauer, P. Rogl, M. Rotter, H. Schmid, F.
Marabelli, A. Devishvili, M. Doerr, G. Giester *J.Phys.: Condens. Matter* **19**
(2007) 216223

[7] N. Melnychenko-Koblyuk, A. Grytsiv, G. Giester, E. Bauer, P. Rogl, M. Rotter, L.
Lackner, L. Fornasari, F. Marabelli *Phys. Rev. B* **76 (**2007) 195124

[8] K.A. Kovnir, A.V. Shevelkov Russian Chemical Review **73** 923 – 938 (2004)

[9] N. Melnychenko-Koblyuk, A. Grytsiv, G. Giester, E. Bauer, P. Rogl, M. Rotter,
G. Durand, H. Kaldarar, R. Lackner, H. Michor, E. Royanian M. Koza *Phys.
Rev. B* **76 (**2007) 144118

[10] N. Melnychenko-Koblyuk, A. Grytsiv G. Giester, St. Berger, H. Kaldarar, H.
Michor, F. Röhrbacher, E. Royanian, E. Bauer, P. Rogl, M. Rotter, H. Schmid,
J.Phys.: Condens. Matter **19** (2007) 046203

[11] W. Carrillo-Cabrera, S. Budnyk, Y. Prots, and Y. Grin *Z. Anorg. Allg. Chem*. **630** (2004) 7226
W. Carrillo-Cabrera, J. Curda, K. Peters, S. Paschen, M. Baenitz, Yu. Grin, H.G.
von Schnering *Z. Kristallogr*. *NCS* **215** (2000) 321
N.L. Okamoto, M.W. Oh, T. Nishii, K. Tanaka, H. Inui *J. Appl. Phys.* **99** (2006)
033513

Tables

table 1: Composition from EPMA and crystallographic data from Rietveld refinement

nominal composition	EPMA (at%)			Accepted composition [a]	Lattice parameter [nm]	Ge2 in 16i (x,x,x)	Ge3 in 24k (0,y,z)
	Ba	Ag	Ge				
$Ba_8Ag_2Ge_{44}$	15.3	4.1	80.6	$Ba_8Ag_{2.1}Ge_{41.9}[]_{2.0}$	1.0743(4)	0.1831(6)	0.1188(3), 0.3149(6)
$Ba_8Ag_3Ge_{43}$	15.3	6.5	78.2	$Ba_8Ag_{3.3}Ge_{41.4}[]_{1.3}$	1.0781(2)	0.1826(4)	0.1173(9), 0.3111(3)
$Ba_8Ag_4Ge_{42}$	14.9	7.7	77.3	$Ba_8Ag_{4.1}Ge_{41.4}[]_{0.5}$	1.0814(2)	0.1827(9)	0.1167(3), 0.3089(9)
$Ba_8Ag_5Ge_{41}$	14.9	8.9	76.2	$Ba_8Ag_{4.8}Ge_{41.2}$	1.0843(1)	0.1826(6)	0.1160(7), 0.3074(3)

[a] from Rietveld refinement

Table 2: phase equilibria and composition from EPMA , X-ray phase analysis and lattice parameter for alloys   annealed at 800°C and annealed at 600°C; a, b, c, d, e, f are for the EPMA images in fig.6

800°C

nominal composition (at%)			X-ray phase analysis	structure type	lattice parameter (Å)			composition EPMA EDX (at%)		
Ag	Ba	Ge			a	b	c	Ag	Ba	Ge
1,85	14,81	83,34	æI	K_4Ge_{23-x}	10,688(0)	10,688(0)	10,688(0)	1,8	15,2	83,0
	a)		æIX	Ba_6Ge_{25}				1,0	18,7	80,3
7,41	14,81	77,78	æI BaGe₂	K_4Ge_{23-x} $BaSi_2$	10,819(4)	10,819(4)	10,819(4)	7,4	14,1	78,5
			æIX	Ba_6Ge_{25}				1,5	18,3	80,2
11,12	14,81	74,07	æI	K_4Ge_{23-x}	10,844(6)	10,844(6)	10,844(6)	9,8	14,6	75,6
			Ba(AgGe)₄	$ThCr_2Si_2$				30,7	19,3	50,0
23,53	5,88	70,59	æI	K_4Ge_{23-x}	10,842(6)	10,842(6)	10,842(6)	9,7	14,5	76,8
	b)		(Ge)	C_{diam}	5,659(7)	5,659(7)	5,659(7)	0,1	0,4	99,5
			liquid							
16,16	33,33	50,51	Ba(AgGe)₂	AlB_2	4,425(3)	4,425(3)	4,880(1)	15,2	32,5	52,3
			Ba(AgGe)₄ BaGe₂	$ThCr_2Si_2$ $BaSi_2$				29,4	23,8	46,8
36	24	40	Ba(AgGe)₂	AlB_2	4,427(1)	4,427(1)	4,882(8)	18,8	29,6	51,6
	c)		Ba(AgGe)₄	$ThCr_2Si_2$	4,610(7)	4,610(7)	10,69(8)	34,2	20,1	45,7
			(Ag)	Cu				0,2	0,3	99,5
25	33	42	Ba(AgGe)₂	AlB_2	4,485(1)	4,485(1)	4,814(3)	21,86	32,98	45,16
			liquid					81,24	16,58	2,18
49,54	10,34	40,12	æI	K_4Ge_{23-x}	10,842(6)	10,842(6)	10,842(6)	10,69	15,17	74,14
	d)		Ba(AgGe)₄	$ThCr_2Si_2$	4,628(5)	4,628(5)	10,64(6)	30,03	20	49,97
			liquid					87,65	0,68	11,67
74,8	15,5	9,7	Ba(AgGe)₂	AlB_2	4,438(6)	4,438(6)	4,868(8)	17,2	33,1	49,7
			liquid					82,1	14,8	3,1
			(Ag)	Cu	4,086(7)	4,086(7)	4,086(7)	96,4	3,1	0,5

600°C

nominal composition (at%)			X-ray phase analysis	structure type	lattice parameter (Å)			composition EPMA EDX (at%)		
Ag	Ba	Ge			a	b	c	Ag	Ba	Ge
1,85	14,81	83,34	æI	K_4Ge_{23-x}	10,805(3)	10,805(3)	10,805(3)	6,6	15,4	78,0
			æIX	Ba_6Ge_{25}	14,560(1)	14,560(1)	14,560(1)	1,6	18,9	79,5
			(Ge)	C_{diam}	5,654(6)	5,654(6)	5,654(6)	0,2	0,3	99,5
7,41	14,81	77,78	æI	K_4Ge_{23-x}	10,819(4)	10,819(4)	10,819(4)	7,4	14,1	78,5
			BaGe₂	$BaSi_2$				0,5	30,7	68,8
	e)		æIX	Ba_6Ge_{25}				1,5	18,3	80,2
16,16	33,33	50,51	Ba(AgGe)₂	AlB_2	4,425(3)	4,425(3)	4,880(1)	15,2	32,5	52,3
			Ba(AgGe)₄ BaGe₂	$ThCr_2Si_2$ $BaSi_2$				29,4	23,8	46,8
14,82	14,82	70,37	æI	K_4Ge_{23-x}	10,844(5)	10,844(5)	10,844(5)	9,7	14,8	75,5
			Ba(AgGe)₄	$ThCr_2Si_2$				29,4	18,9	51,7
25	33	42	Ba(AgGe)₂	AlB_2	4,488(8)	4,488(8)	4,808(8)	22,7	32,4	44,9
			Ba(AgGe)₅	$CaCu_5$	5,819(0)	5,819(0)	4,599(5)	79,5	16,5	4,0
29,75	13,67	56,58	æI	K_4Ge_{23-x}	10,840(9)	10,840(9)	10,840(9)	8,6	15,2	76,1
			Ba(AgGe)₄	$ThCr_2Si_2$	4,614(0)	4,614(0)	10,680(9)	29,4	20,8	49,8
			(Ag)	Cu				93,6	0	62
36	24	40	Ba(AgGe)₂	AlB_2	4,427(2)	4,427(2)	4,882(3)	18,2	32,7	49,1
			Ba(AgGe)₄	$ThCr_2Si_2$	4,605(9)	4,605(9)	10,711(7)	32,0	21,1	46,9
			(Ag)	Cu	4,089(1)	4,089(1)	4,089(1)	95,6	0	4,4
23,53	5,88	70,59	æI	K_4Ge_{23-x}	10,842(6)	10,842(6)	10,842(6)	9,7	14,1	76,2
	f)		(Ge)	C_{diam}	5,659(7)	5,659(7)	5,659(7)	0,3	0,4	99,3
			(Ag)	Cu				88,6	0,3	11,1

table 3: results from DSC measurements

sample	phase 1	phase 2	phase 3	T solidus (°C)	T liquidus (°C)	T other signal (°C)
D5 800	Clathrate I	(Ge)	-	~ 812	856 ± 0,5	637 ± 2
						841,6 ± 0,5
A1 600	Clathrate I	Clathrate IX	(Ge)	813,4 ± 1	825 - 835	715 ± 5
						819,2 ± 1
B6 600	Clathrate I	Ba(AgGe)$_2$	-	775 ± 1	863 ± 2	638 ± 3
						821 ± 2
C4 600	Ba(AgGe)$_4$	Ba(AgGe)$_2$	(Ag)	861 ± 3	893 ± 1	~ 648
						~ 697
A7 600	Clathrate I	(Ge)	(Ag)	637 ± 1	816 ± 1	~ 707
C2 600	Ba(AgGe)$_4$	Ba(AgGe)$_2$	BaGe$_2$	886 ± 2	897± 1 reaction with crucible!	~ 815

Figures
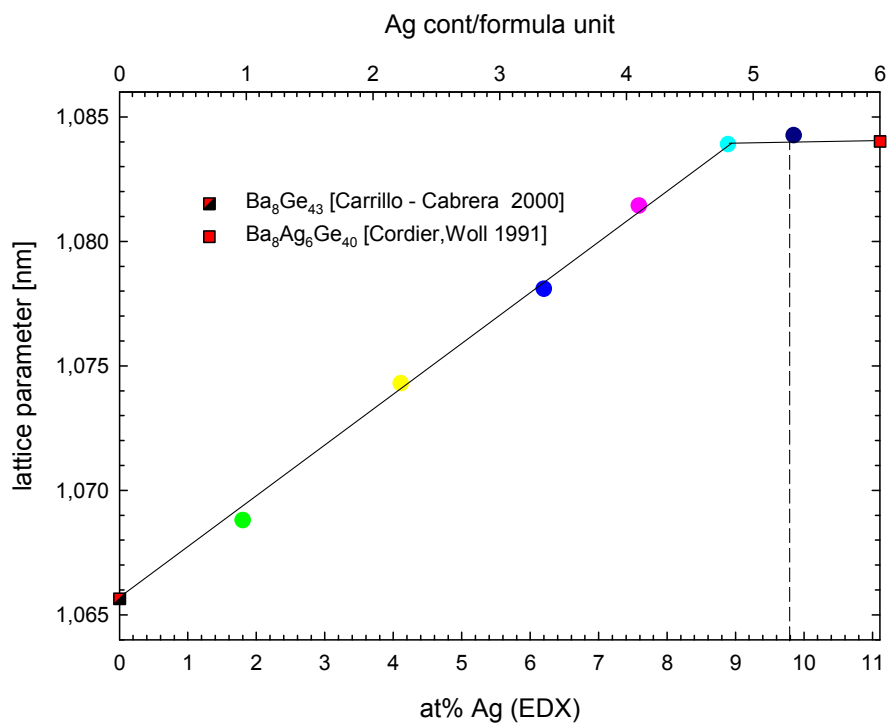
Fig. 1: lattice parameter (Å) vs. silver content for Ba$_8$Ag$_x$Ge$_{46-x}$ (x = 1,2,3,4,5)
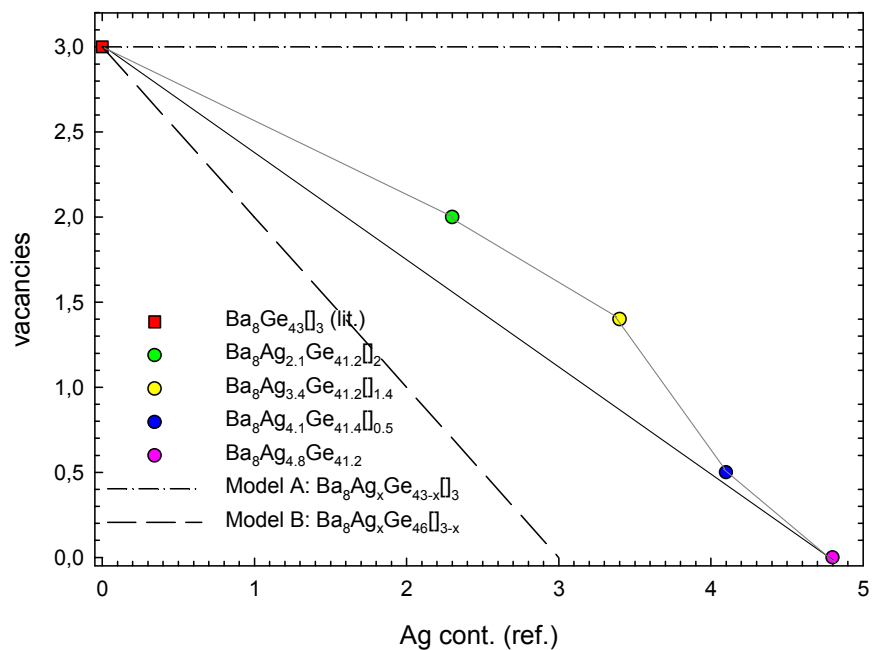
Fig. 2: Concentration of vacancies vs. silver content per formula unit
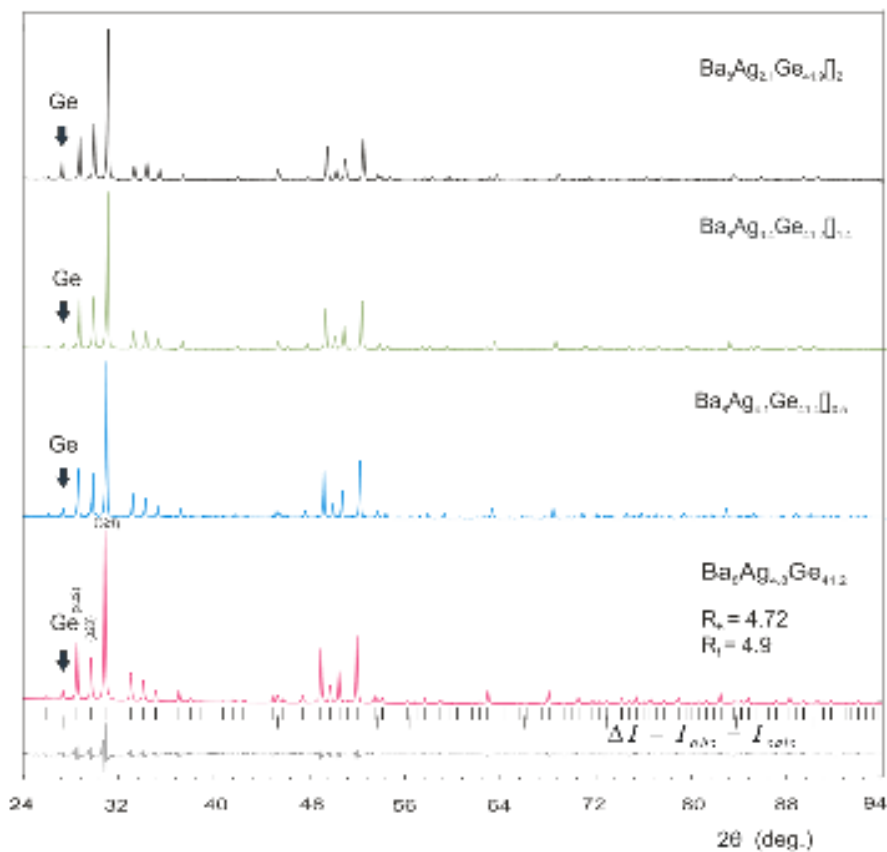
Fig. 3: XRPD pattern and Rietveld refinement for $Ba_8Ag_xGe_{46-x-y}\square_y$ (x = 2.1, 3.4, 4.1 and 4.8)
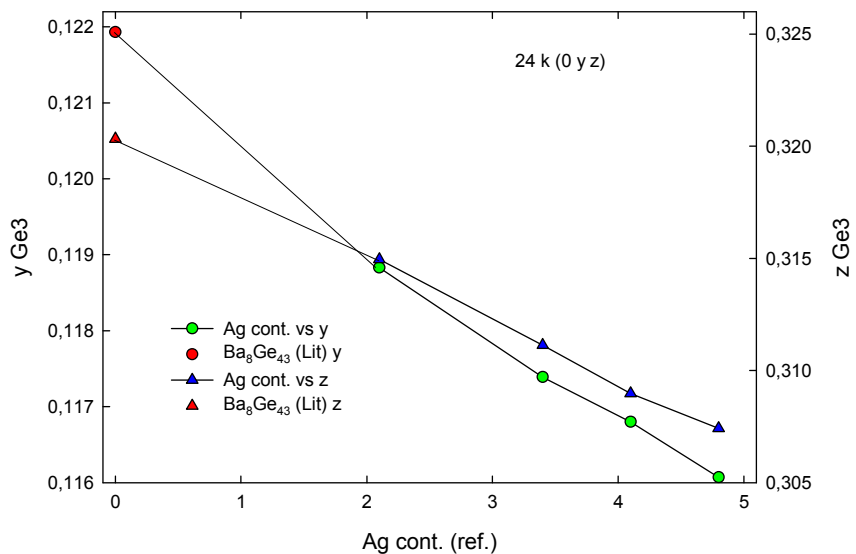
Fig. 4: Ag content/formula unit vs. compositional parameters y and z for the Ge3 site (0, y, z)
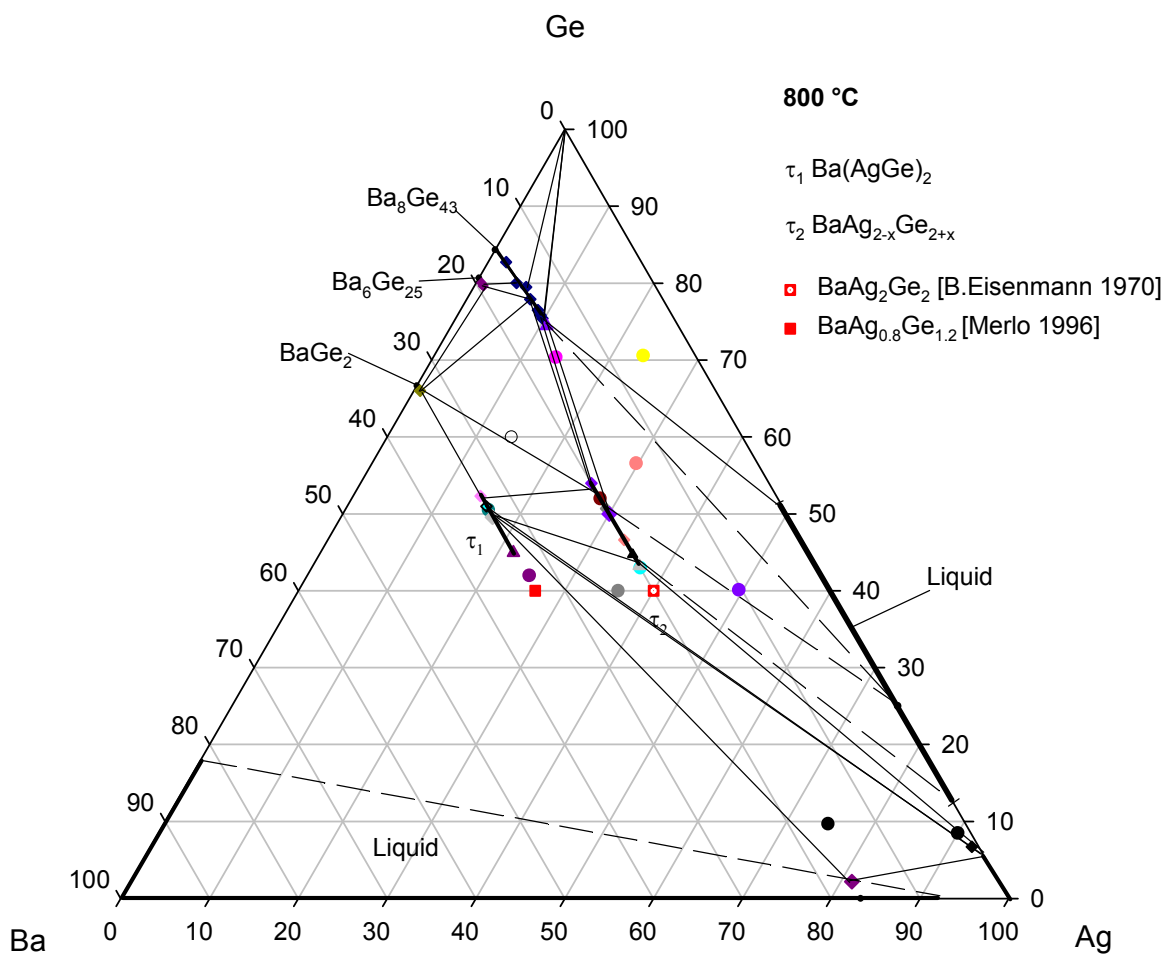
Fig. 5: partial isothermal section at 800°C in the ternary Ba – Ag - Ge system
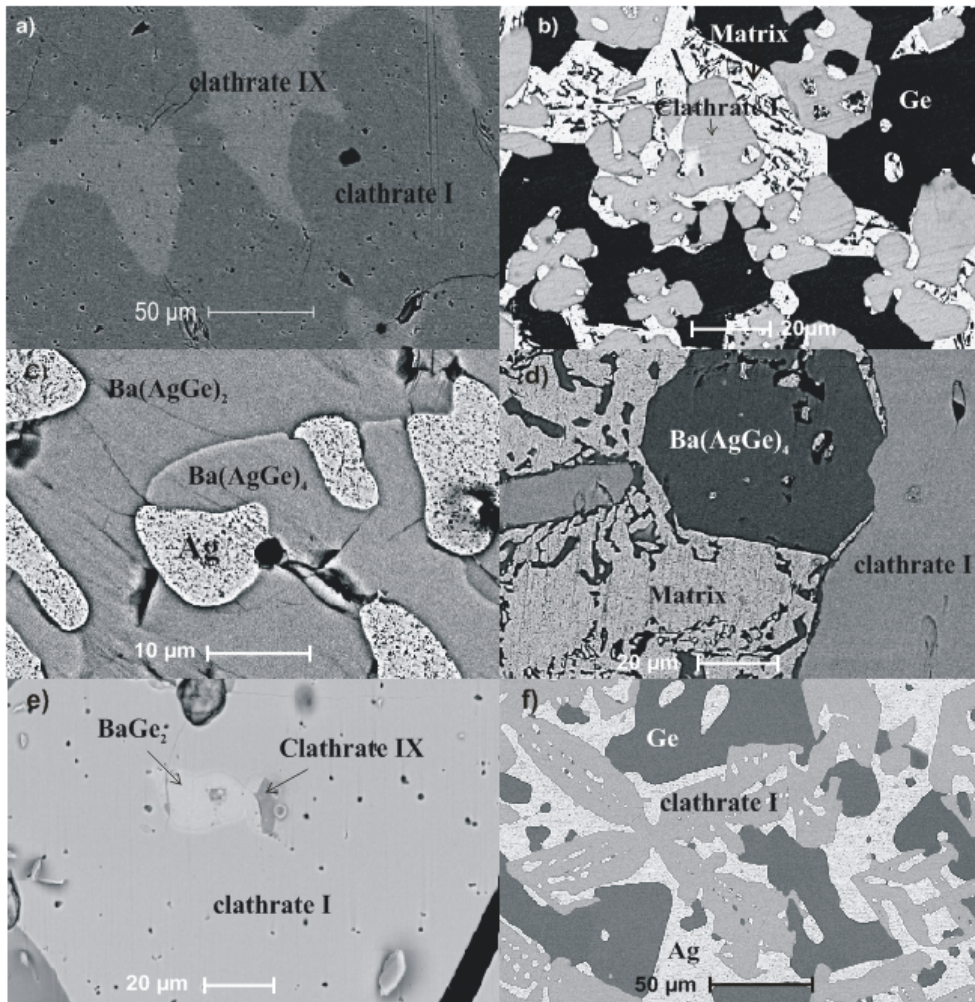
Fig. 6: microstructures of several Ba – Ag – Ge alloys annealed at 800°C: a), b), c), d) and annealed at 600°C: e), f). Nominal composition, atomic percent from EPMA and X-ray phase analysis are given in table 2.
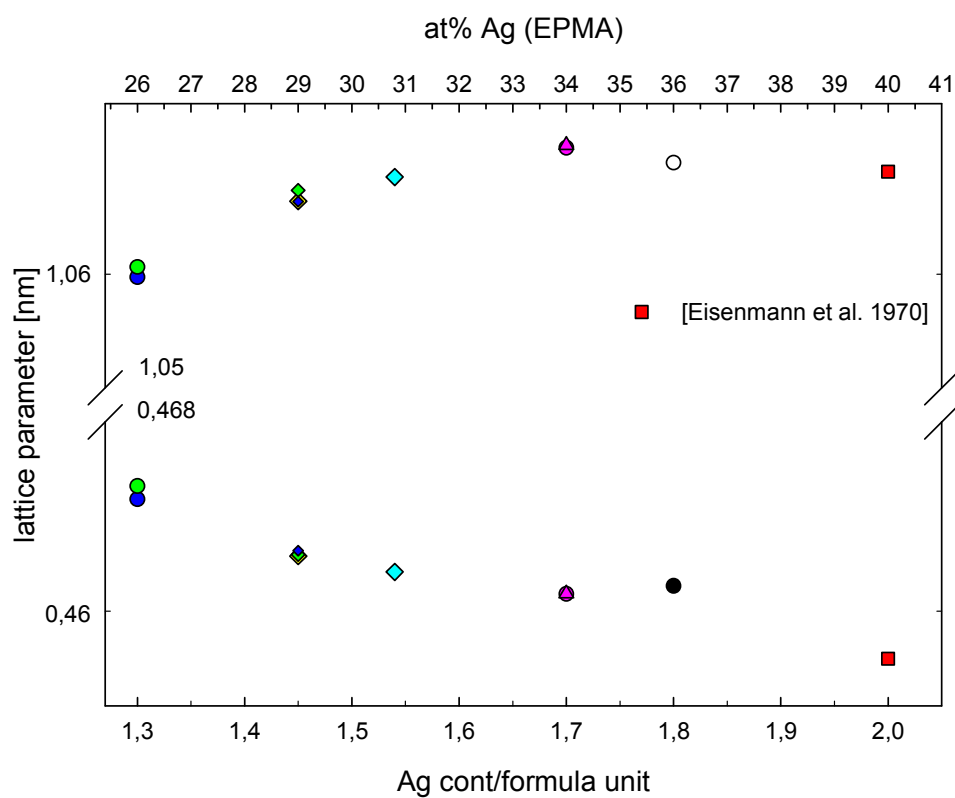
Fig. 7: dependency of the lattice parameter of the silver content for BaAg$_{2-x}$Ge$_{2+x}$
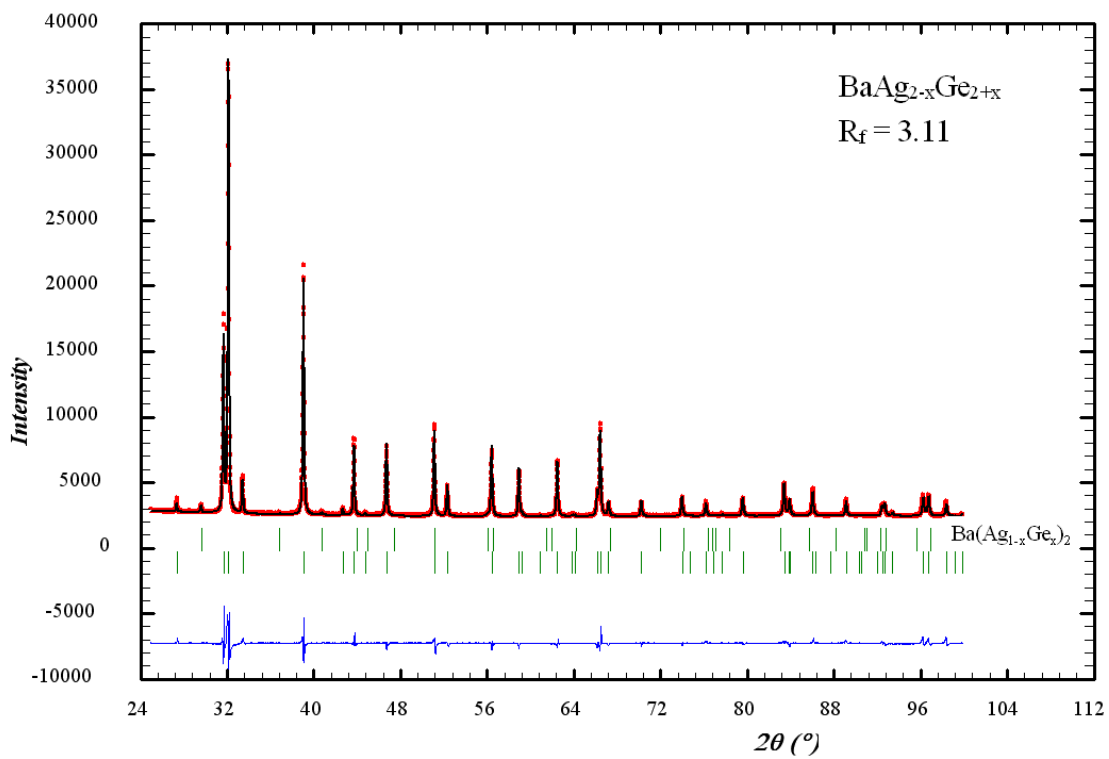
Fig.8: Rietveld refinement for BaAg$_{2-x}$Ge$_{2+x}$ (x=0.2, ThCr$_2$Si$_2$ structure type, R$_f$ = 3.11, z4e=0.3819(5)) as the main phase
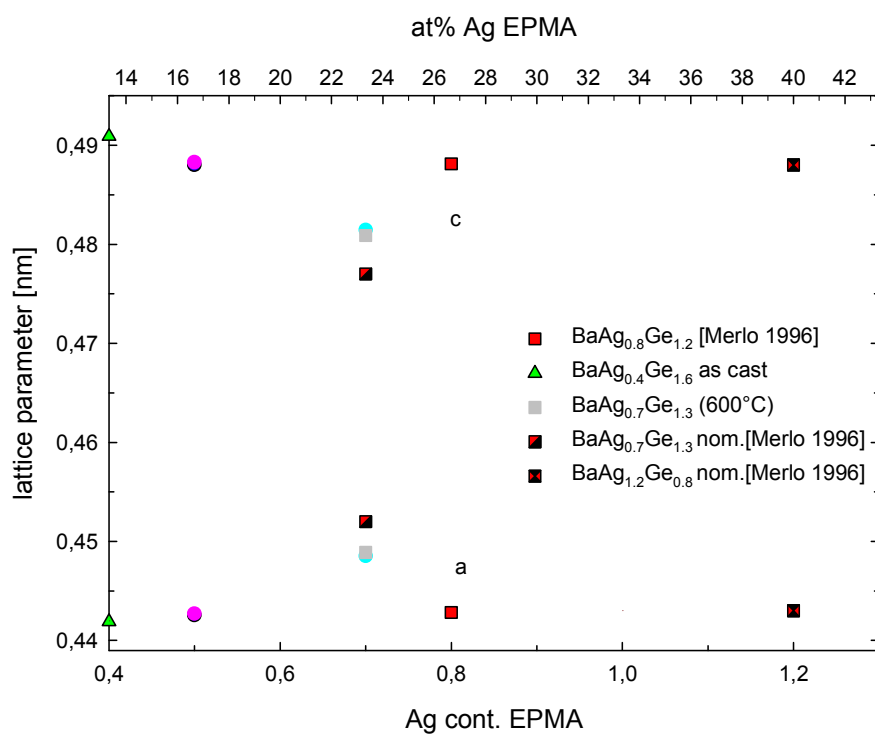
Fig. 9: lattice parameter vs. silver content for Ba(Ag$_{1-x}$Ge$_x$)$_2$
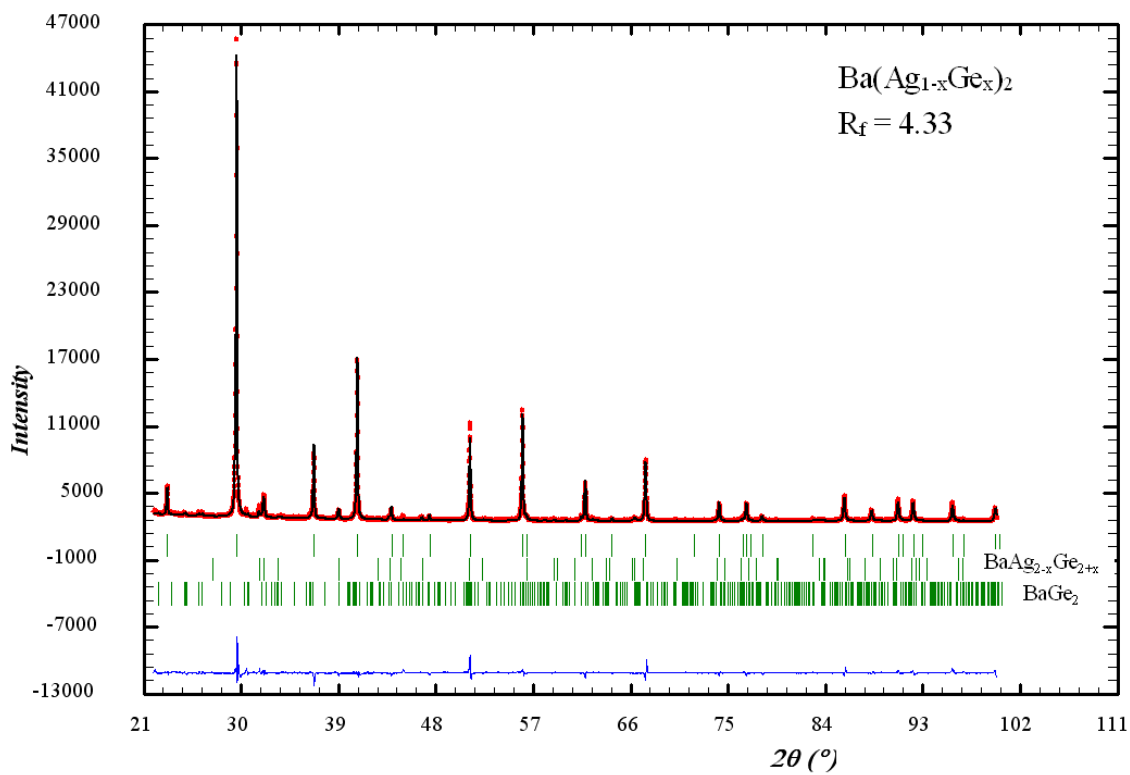
Fig. 10: Rietveld refinement for Ba(Ag$_{1-x}$Ge$_x$)$_2$ (AlB$_2$ structure type, x=0.65, Rf = 4.33) as the main phase.
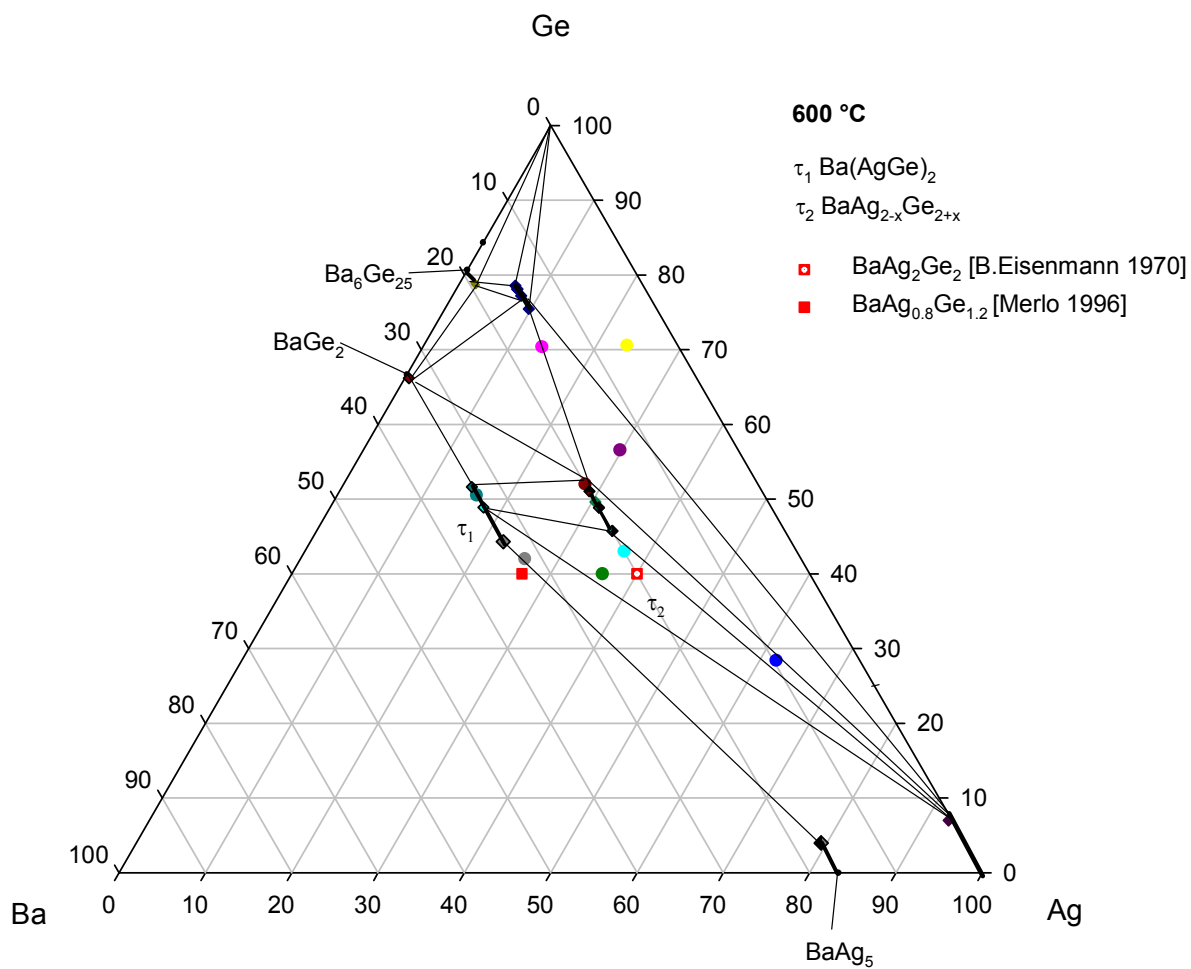
Fig. 11: partial isothermal section at 600°C of the ternary system Ba – Ag – Ge
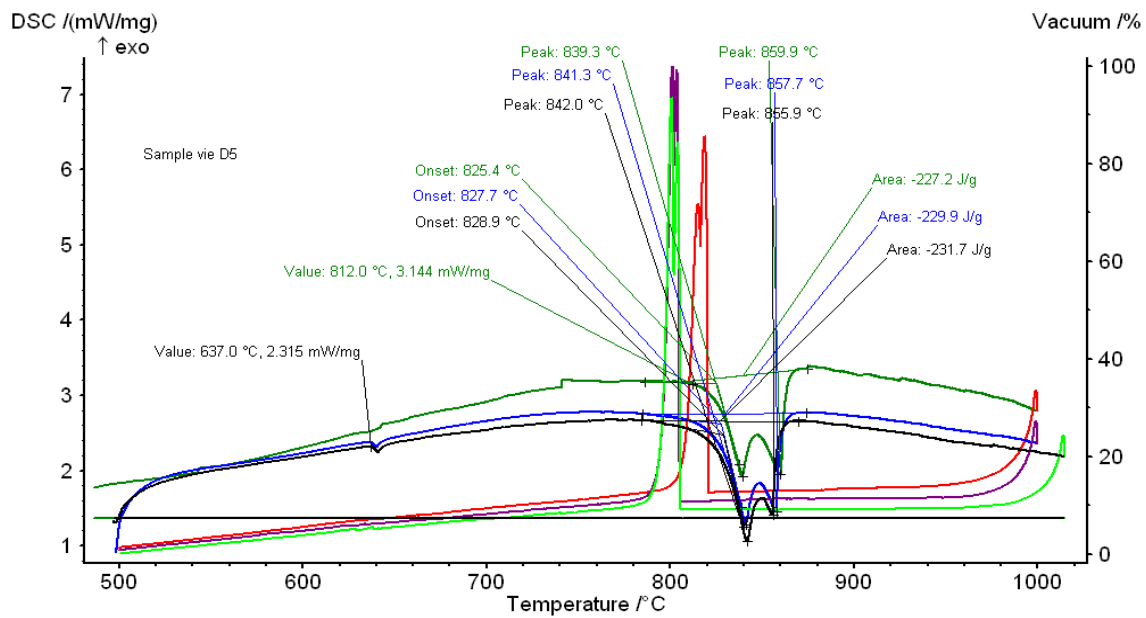
Fig. 12: DSC signals for Ba$_8$Ag$_{4.8}$Ge$_{41.2}$ (+Ge)

The Ba – Ag - Si system

INTRODUCTION

Despite superconductivity, discovered in Na and Ba doped silicon clathrates [2,3], triggered intense studies of clathrate type I compounds $Ba_8Ag_xSi_{46-x}$ [4,5,6], there is still little known about phase equilibria in the ternary Ba – Ag – Si system and about the homogeneity region of clathrates at a defined temperature.

Electronic band structure calculations of Ba_8Si_{46} and $Ba_8Ag_6Si_{40}$ were combined with photoemission experiments performed on arc melted alloys $Ba_8Ag_xSi_{46-x}$ (x=0,1,3,6), which were ground and compressed at 3 GPa and 800 °C in an h-BN container [5].

Single crystal X-ray data confirmed Ag atoms in the 6c-site of the clathrate type I structure (Pm-3n, [7]), without superstructure formation in contrast to binary $Ba_8Ge_{43}\square_3$ with a 8-fold enlargement of the basic clathrate type I unit cell.

Besides the clathrate type-I compound, a further ternary compound has been reported in literature. Dörrscheidt and Schäfer [9] mentioned a compound without large homogeneity region found from nominal compositions $BaAg_xSi_{2-x}$ ($0.5 \leq x \leq 1.0$, space group C222, a=0.862(1), b=1.493(2), c=1.965(2) nm, presumably $Sr_8Ag_5Si_9$-type as a derivative of the AlB_2-type). Single crystal X-ray intensity refinements by Merlo et al. [10] prompted a composition $Ba_{32}Ag_{21.54}Si_{30.2}$ ($Ba_3Ag_2Si_3$ structure type, C222, lattice parameters similar to [9]). A more recent reinvestigation by R. Cardoso Gil et al. [11] arrived at a formula $Ba_4Ag_2Si_6$ with slightly different space group ($Ba_4Li_2Si_6$ structure type, Fddd, a = 0.862, b = 1.493 and c = 1.965 nm) but with the same lattice geometry for a superstructure of the AlB_2-type according to (a = 2 a_{AlB2}, b = 2$\sqrt{3}$ a_{AlB2}, c = 4 c_{AlB2}).

EXPERIMANTAL DETAILS

The samples (~1g) for the isothermal section at 800°C were prepared by arc melting from the pure elements (Ba 99.9, Ag 99.9 and Si 99.9999 mass%) under an argon atmosphere. The weight loss was in all cases lower then 1 mass%. After arc melting they were sealed in quartz tubes under vacuum and annealed at 800°C for at least 1 week. For the characterisation of the samples, X-ray powder diffraction (XRPD), electron probe microanalysis (EPMA) and differential thermal analysis (DTA) were used. In all cases, for X-ray powder diffraction, a Guinier-Huber image plate recording system (monochromatic $CuK\alpha_1$ radiation) was employed and lattice parameters were calculated by least-square fits using Ge or Si as internal standard (a_{Ge} = 0.565791 and a_{Si} = 0.543106 nm). Rietveld refinements were made with the FULLPROF program [12]. To image the microstructure of the samples a Philips XL 30 ESEM-FEG (emission environmental scanning electron microscope)

was used and the chemical composition was determined with electron probe microanalysis (EDX detector) using Buehler Simplimett 3 and JSM 6400 SEM equipment. Differential thermal analysis was carried out in a STA 409 Netzsch differential scanning calorimeter with a heating rate of 10 K/min (5, 1, 0.1 K/min if necessary) in Y_2O_3 protective coated Al_2O_3 crucibles under an argon stream (6N, 70 ml/min) to find the liquidus temperature of the clathrate.

One sample with nominal composition $Ba_8Ag_5Si_{41}$ was prepared in a different way to reach high density for physical property measurements (thermopower, resistivity and thermal conductivity). For each sample of about 1 cm³, 5 smaller samples with a weight of 1-2g were prepared by arc melting from the pure elements under an argon atmosphere. After arc melting they were sealed under vacuum into quartz tubes and annealed for 5 days at 800°C. For powdering a ball mill (Vario Planetenmühle, Pulverisette 4) was used. The resulting powders were compacted in a hot press (HP W 200/250-2200-200-Ks, FCT System GmbH) by 800°C and a pressure of 4kN under an argon atmosphere followed by annealing in sealed quartz tubes at 800°C for 1 week.

RESULTS AND DISCUSSION

The solid solution for clathrate type I $Ba_8Ag_xSi_{46-x}$

The solubility range of the ternary type-I clathrate at 800 °C was studied by XRPD and EPMA on a series of samples with nominal composition $Ba_8Ag_xSi_{46-x}$ (x = 3,4,5,6). Table 1 shows a comparison of the EPMA data with the results of Rietveld refinement of the X-ray spectra. In all cases the spectra could be fully indexed in the basis of a cubic clathrate type I lattice (space group P m-3n) with minor amounts of Si. As no binary clathrate type I exists under normal pressure the ternary homogeneity region is very limited at 800°C and was found to extend from $Ba_8Ag_{4.3}Si_{41.7}$ to $Ba_8Ag_{5.4}Si_{40.6}$ (Fig. 1). The lattice parameters show a linear increase with increasing silver content but differ quite strongly from those reported by Cordier at al.[7] (X-ray single crystal data, a = 1.0478(6) nm for $Ba_8Ag_{3.8}Si_{42.2}$) and Rüdiger F.W. Herrmann et al. [6] (XRPD, a = 1.045 nm for $Ba_8Ag_4Si_{42}$).

Figure 2 shows the XRPD pattern of the clathrate series with increasing silver content and the Rietveld refinement for one of them. The refinement unambiguously located the Ba atoms in the 2a (0, 0, 0) and 6c $(\frac{1}{4},0,\frac{1}{2})$ sites, Ag and Si atoms can be found in the 6d $(\frac{1}{4},\frac{1}{2},0)$ site. The Ag content was fixed from EPMA measurements. Silicon occupies the 16i (x, x, x) and 24k (0, y, z) sites. Although Cordier et al. [7] reported that Ag preferentially occupies the 6c site our refinement showed for all samples, that minor amounts of Ag also occupy the 24k site. No vacancies were encountered. The sample with the lowest silver content contains beside silicon a small amount of $BaSi_2$ and the other samples contain less than 10% of a second phase (Si). Substitution of silicon

atoms with silver atoms in the crystal lattice does not lead to largely different x in the 16i site (x, x, x) whilst small changes of the coordinates of the Si3 atoms in the 24k site (0, y, z) are observed. The positional parameter y and z of the 24k site, decreases with increasing silver content (Fig. 3). It should be mentioned here that the positional parameters for the Si3 site according to the structure determination by Cordier [7] and our data show a similarly large discrepancy as the lattice parameters.

Phase equilibria in the system Ba – Ag – Si for 0 to 33.3 at.% Ba.

The isothermal section at 800°C for the silicon and silver rich part is shown in figure 4. At low Ag content, clathrate I is in equilibrium with silicon and $BaSi_2$. At higher silver content, the equilibrium phase was identified as τ_2-$Ba_4Ag_2Si_6$ ($Ba_4Li_2Si_6$ structure type), which does not show a homogeneity range at 800 °C and oxidizes on air. The Rietveld refinement for $Ba_4Ag_2Si_6$, is shown in Fig. 5. The second phase is $BaAg_5$, which actually is liquid at 800°C. The experimental results from Rietveld refinement and EPMA are combined in table 2 and figure 6. For some phases it was not possible to calculate lattice parameter because the XRPD peaks were too weak or were overlapping quite strong. Fig. 6 shows the SEM images of the samples documenting the three-phase equilibria at 800°C. It is interesting to note that high pressure synthesis at 3 GPa, 800°C yields a continuous clathrate type I solid solution starting from binary Ba_8Si_{46} up to $Ba_8Ag_6Si_{40}$ at surprising and significantly larger unit cell parameters [a = 1.0560 nm].

Analysis of the ball-milled and hot pressed sample $Ba_8Ag_5S_{41}$

For the characterization of the ball milled-hot pressed sample, as already mentioned, X-ray powder diffraction and EPMA for phase determination were used. Rietveld refinement of the powder pattern of the sample shows small amounts (~2.3%) of silver as a secondary phase. This is in good agreement with the results from EPMA (fig. 7). The results from EPMA and Rietveld refinement are summarized in table3. DTA investigations were made to find the liquidus temperature for this sample, (fig. 8) revealing a value of about 1141°C.

References

[1] C. Cros, M. Pouchard, P. Hagenmuller, *C. R. Acad. Sci. Paris* **260** (1965) 4764.
    S. Kasper, P. Hagenmuller, M. Pouchard, C. Cros, *Science* **150** (1965) 1713.
    C. Cros, M. Pouchard, P. Hagenmuller, *J. Solid State Chem.* **2** (1970) 570.

[2] H. Kawai, H. O. Horie, S. Yamanaka and M. Ishikawa, *Phys.Rev.Lett.* **74**, 1427
    (1995)

[3] S.Yamanaka, E. Enishi, H. Fukuoka and M. Yasukawa, *Inorg. Cem.* **39**, 56 (2000)

[4] J.S. Tse, T. Itaka, T.Kume and H. Shimizu, K. Parlinski, H. Fukuoka and S.
    Yamanaka *Phsical Review B* **72**, 155441 (2005)

[5] N. Kamakura, T. Nakano, Y. Ikemoto, M. Usuda, H. Fukuoka, S. Yamanaka, S. Shin,
K.Kobayashi *Phsical Review B* **72,** 014511, 2005

[6] R.F.W. Herrmann, K. Tanigaki, S. Kuroshima, H. Suematsu *Chemical Physical
    Letters* **283,** 29-32 (1998)

[7] Cordier and Woll, *J. Less-Common. Met.* **169**, 291 (1991)

[8] K.A. Kovnir and A.V. Shevelkov, *Russian Chemical Review* **73**, 923 (2004)

[9] W. Dörrscheidt and H.Schäfer, *Journal of the Less-Common. Metals* 78, 69 – 79
    (1981)

[10] F. Merlo, M.L. Fornasini *Journal of Alloys and Compounds* **232,** 289 (1996)

[11] R. Cardoso Gil, W. Carrillo-Cabrera, M.Schultheiss, K. Peters, H. G. von
     Schnering *Z. anorg. allg. Chem.*, **625**, 285 (1999)

[12] J. Rodriguez-Carvajal, FULLPROF, Abstract of the satellite meeting on powder
     diffraction of the 15 congress, Int. Union of Crystallography, Talence, 127 (1990)

Tables

Table 1: results from EPMA and Rietveld refinement for $Ba_8Ag_xSi_{46-x}$

Nominal composition	EPMA (at%)			Accepted composition[a]	Lattice parameter [Å]	Si2 in 16i (x,x,x)	Si3 in 24k (0,y,z)
	Ba	Ag	Si				
$Ba_8Ag_3Si_{43}$	15.3	8.4	76.3	$Ba_8Ag_{4.3}Si_{41.7}$	10.4309(3)	0.1832(4)	y=0.1170(4), z=0.3058(6)
$Ba_8Ag_5Si_{41}$	15.8	10.0	74.2	$Ba_8Ag_5Ge_{41}$	10.4585(1)	0.1833(2)	0.1153(7), 0.3050(6)
$Ba_8Ag_6Si_{40}$	15.2	10.3	74.5	$Ba_8Ag_{5.4}Ge_{40.6}$	10.4613(5)	0.1842(2)	0.1149(2), 0.3049(6)

[a] from Rietveld refinement

Table 2: EPMA and X-ray phase analysis data for ternary alloys (quenched from 800°C) in the system Ba-Ag-Si; a, b, c, and d correspond to the SEM images of figure 6

nominal composition (at%)			X-ray phase analysis	structure type	lattice parameter (Å)			composition EPMA (EDX) (at%)		
Ag	Ba	Si			a	b	c	Ag	Ba	Si
5,56	14,81	79,63	(Si)	C_{diam}	5,431(4)	5,431(4)	5,431(4)	0	0	100
a)			τ_1 BaSi$_2$	K$_4$Ge$_{23-x}$ BaSi$_2$	10,430(9)	10,430(9)	10,430(9)	8,2 / 0,5	15,7 / 33,3	76,2 / 66,2
7,41	14,81	77,78	Ba$_4$Ag$_2$Si$_6$	Ba$_4$Li$_2$Si$_6$				16,3	33,1	50,6
c)			τ_1 BaSi$_2$	K$_4$Ge$_{23-x}$ BaSi$_2$	10,440(3)	10,440(3)	10,440(3)	9,3 / 0,7	15,7 / 33,6	75,1 / 65,8
23,53	5,88	70,59	(Si)	C_{diam}	5,431(0)	5,431(0)	5,431(0)	0	0	100
b)			(Ag)	Cu	4,09(25)	4,09(25)	4,09(25)	96,48	0	3,52
			τ_1	K$_4$Ge$_{23-x}$	10,459(9)	10,459(9)	10,459(9)	10,28	15,49	74,23
64,3	7,1	28,6	τ_1	K$_4$Ge$_{23-x}$	10,461(3)	10,461(3)	10,461(3)	10,3	15,2	74,5
			(Ag)	Cu	4,081(9)	4,081(9)	4,081(9)	96,7	3,3	0,0
			Ba$_4$Ag$_2$Si$_6$	Ba$_4$Li$_2$Si$_6$				16,5	31,6	51,9
33,33	33,33	33,34	Ba$_4$Ag$_2$Si$_6$	Ba$_4$Li$_2$Si$_6$	8,61(25)	14,92(01)	19,64(30)	17,73	34,23	48,04
d)			liquid					0,5	84,31	15,19

Table 3: results from EPMA and Riedveld refinement

Nominal composition	EPMA (at%)			Accepted composition[a]	Lattice parameter nm
	Ba	Ag	Si		
Ba$_8$Ag$_5$Ge$_{41}$	15.8	10.0	74.2	Ba$_8$Ag$_5$Ge$_{41}$	1.04585(1)

Figures

Ag cont./formula unit

■ Ba$_8$Ag$_{3.8}$Si$_{42.2}$ [Cordier,Woll 1995]
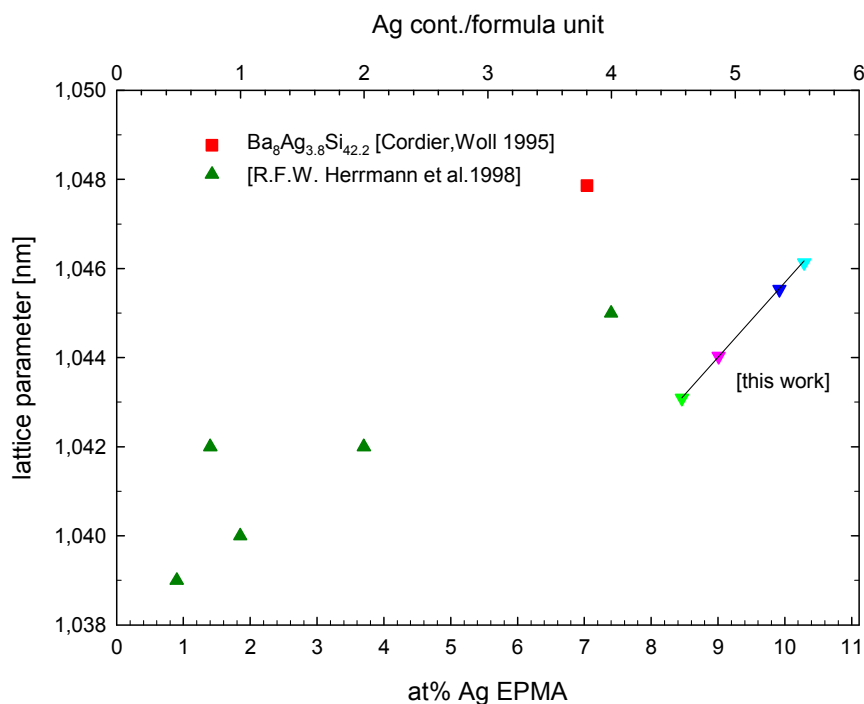▲ [R.F.W. Herrmann et al.1998]

[this work]

Fig.1: Lattice parameters versus silver content for alloys Ba$_8$Ag$_x$Si$_{46-x}$, quenched from 800°C and literature data
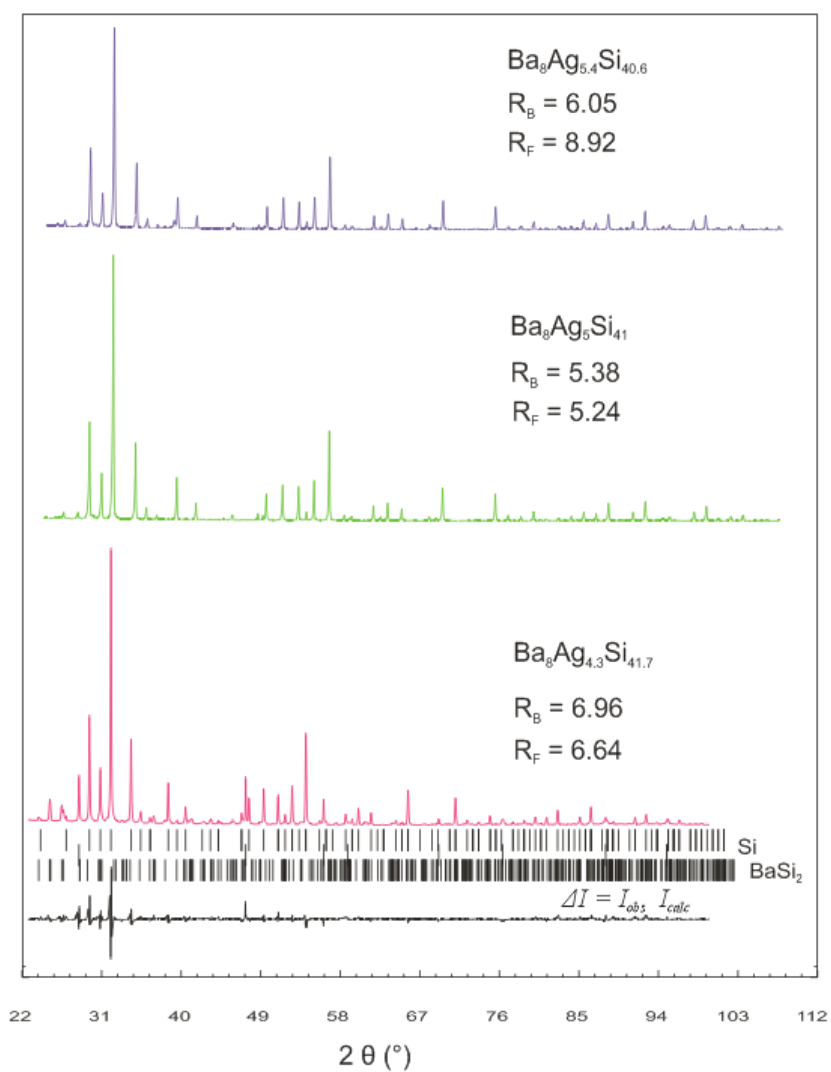
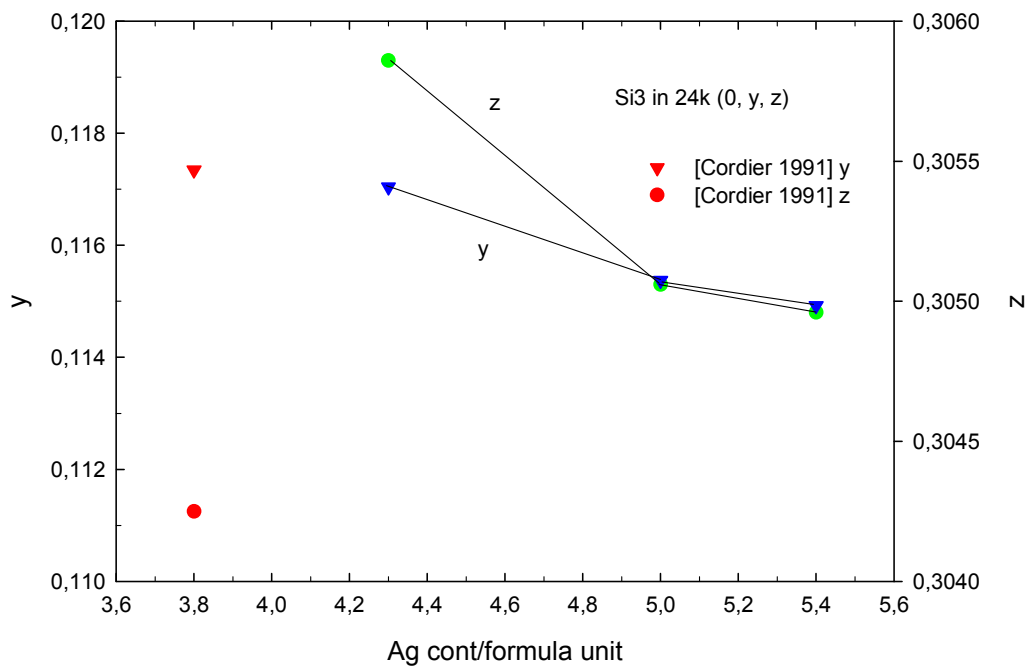Fig.2: XRPD pattern and Rietveld refinement for various alloys $Ba_8Ag_xSi_{46-x}$

Fig.3: Ag content per formula unit vs. compositional parameters y and z for the Si3 site (24k (0, y, z))
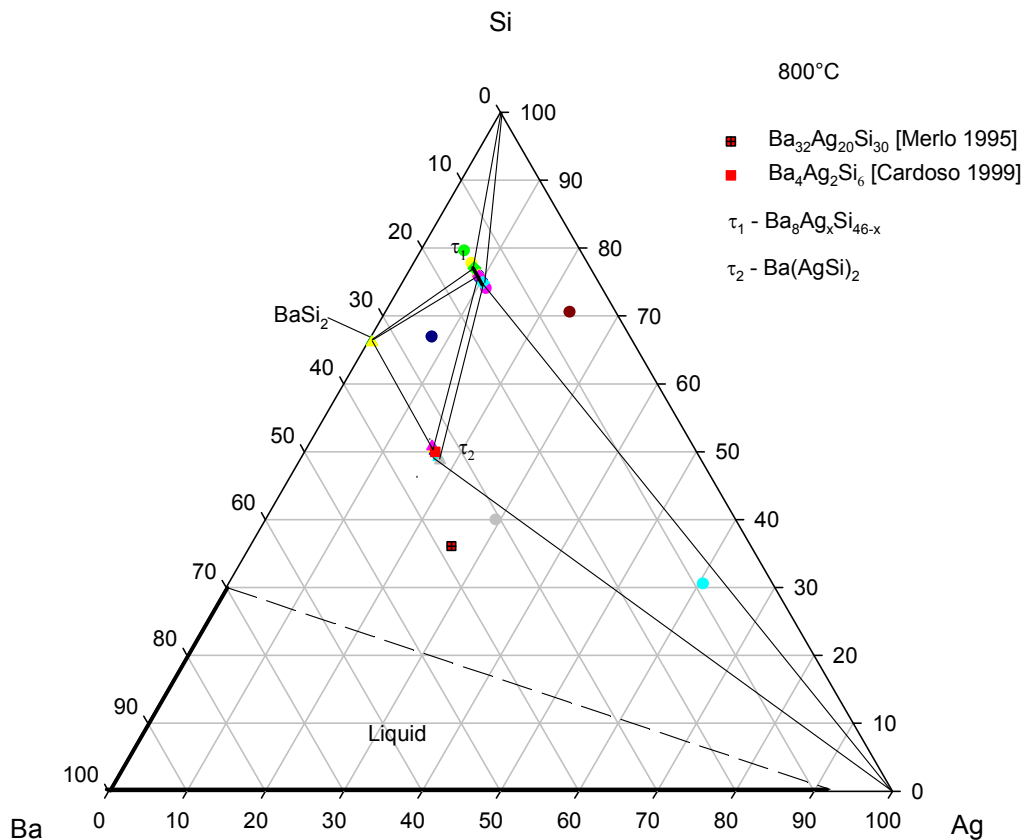

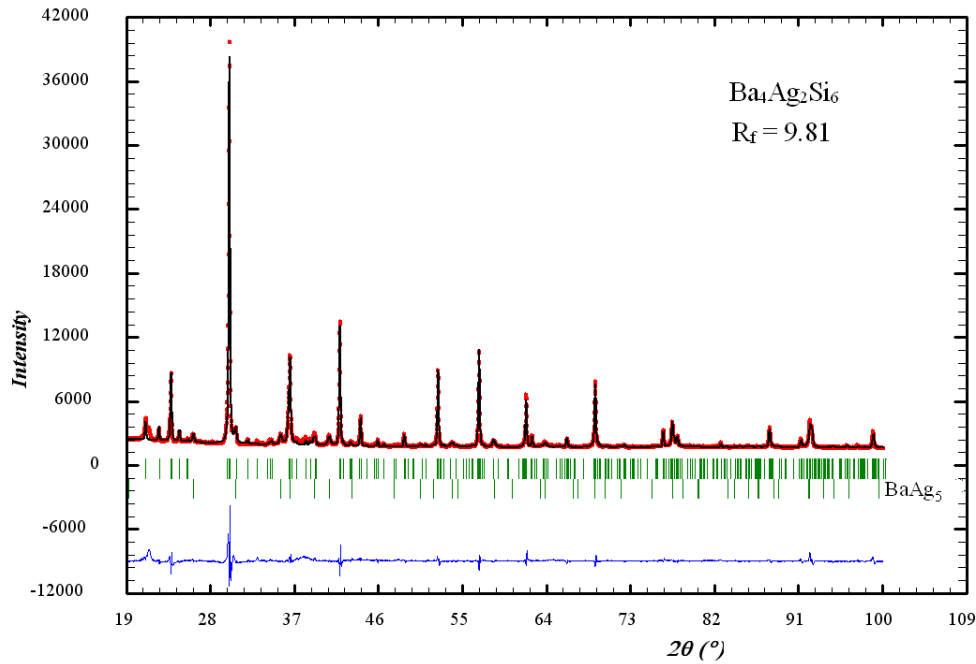Fig.4: Partial isothermal section for the ternary system Ba – Ag – Si at 800°C.

Fig.5: Rietveld refinement for a sample containing $Ba_4Ag_2Si_6$ (a = 0.861(2), b = 1.492(0),
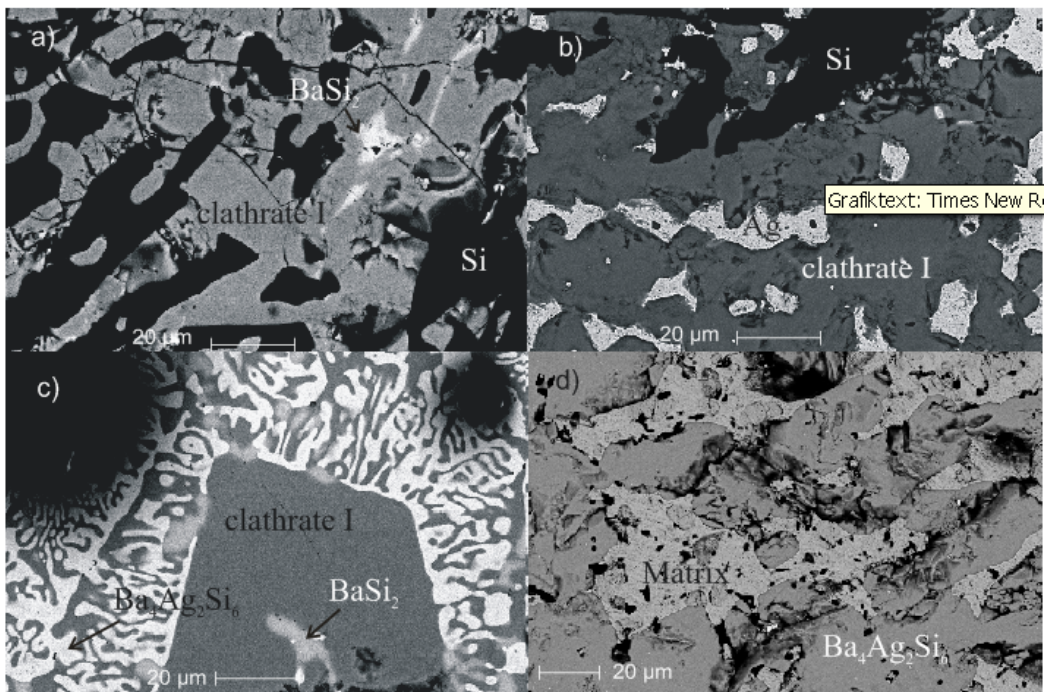
c = 1.964(3) nm); $BaAg_5$ is in liquid state at 800°C

Fig. 6: SEM images showing the microstructures of several alloys Ba – Ag – Si annealed at 800°C; the

phase compositions of a, b, c, d can be found from table 2
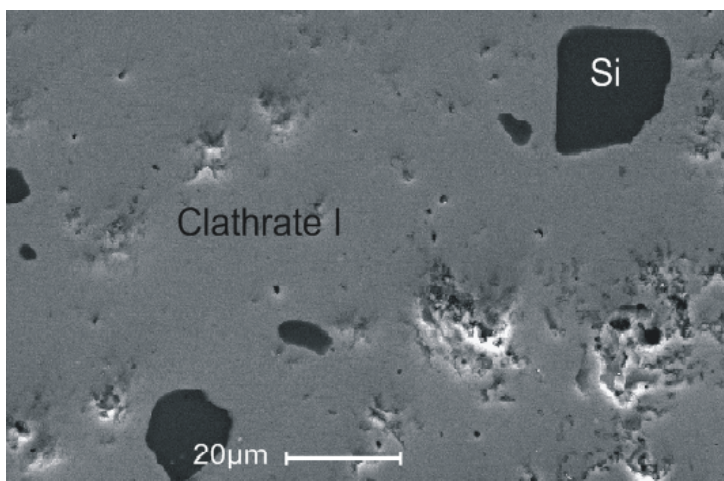
Fig. 7: SEM images of $Ba_8Au_6Ge_{40}$
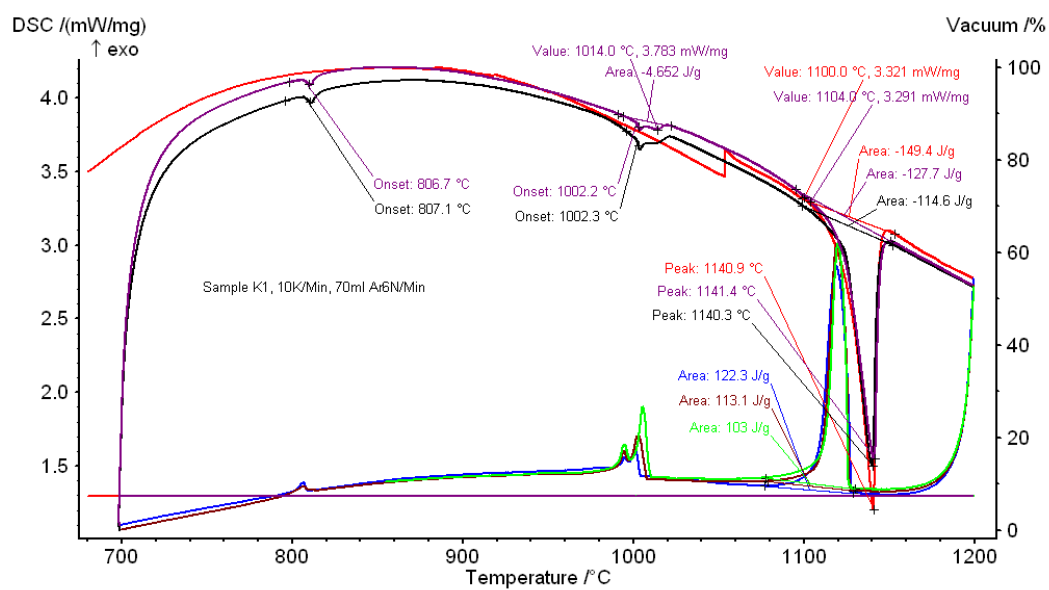
Fig. 12: DSC signals for $Ba_8Ag_5Si_{41}$

The Ba – Au – Si system

INTRODUCTION

Since the discovery of superconductivity in Na and Ba doped silicon clathrates of type-I [2,3], the clathrates $Ba_8Au_xSi_{46-x}$ have been studied intensively. Single crystal X-ray refinements proved isoypism with the clathrate type I structure for three alloys $Ba_8Au_xSi_{46-x}$, x = 5.4, 5.9 [5] and 6.0 [6]. In contrast to the data by Cordier [8] suggesting full atom order with Au atoms in the 6c sites, the investigation by Jaussaud et al. [5] revealed a lower gold content within the 6c sites, but a small random substitution of Au for Si within the 24k sites. Thermoelectric properties and ^{29}Si MAS NMR spectroscopy indicated that the two samples x = 5.4, 5.9 were either n-type or p-type materials, respectively [5]. The maximum superconducting fraction in the clathrate solution $Ba_8Au_xSi_{46-x}$ ($0.2 \leq x \leq 6$) prepared at 800°C under 3 GPa was found at x = 1 [4]. Electronic structure calculations confirmed the metallic character of $Ba_8Au_6Si_{40}$ for which TEM studies confirmed the simple type I unit cell (space group Pm-3n) [7]. DFT calculations are due Tse et al. [6]. Besides the type I clathrate, the formation of layered structures and the high temperature and high pressure synthesis of $BaAu_2Si_2$ ($ThCr_2Si_2$ structure type, a = 0.45331(6) and c = 1.0297(1) nm) has been reported [9].

EXPERIMANTAL DETAILS

The samples (~1g) for the isothermal section at 800°C were prepared by arc melting from the pure elements (Ba 99.9, Au 99.9 and Si 99.9999 mass%) under an argon atmosphere. The weight loss was in all cases lower then 1 mass%. After arc melting they were sealed in quartz tubes under vacuum and annealed at 800°C for at least 1 week. For the characterisation of the samples, X-ray powder diffraction (XRPD), electron probe microanalysis (EPMA) and differential thermal analysis (DTA) were used. In all cases, for X-ray powder diffraction, a Guinier-Huber image plate recording system (monochromatized CuKα$_1$ radiation) was employed and lattice parameters were calculated by least-square fits using Ge or Si as internal standard (a_{Ge} = 0.565791 and a_{Si} = 0.543106 nm). Rietveld refinements were made with the FULLPROF program [10]. To image the microstructure of the samples a Philips XL 30 ESEM-FEG (emission environmental scanning electron microscope) was used and the chemical composition was determined with electron probe microanalysis (EDX detector) using Buehler Simplimett 3 and JSM 6400 SEM equipment. Differential thermal analysis was carried out in a STA 409 Netzsch differential scanning calorimeter with a heating rate of 10 K/min (5, 1, 0.1 K/min if necessary) in Y_2O_3 protective coated Al_2O_3 crucibles under an argon stream (6N, 70 ml/min) to find the liquidus temperature of the clathrate.

One sample with nominal composition $Ba_8Au_5Si_{41}$was prepared differently to reach a higher density

for physical property measurements (thermopower, resistivity and thermal conductivity). For each sample of about 1 cm³, 5 smaller samples with a weight of 1-2g were prepared by arc melting from the pure elements under an argon atmosphere. After arc melting they were sealed under vacuum into quartz tubes and annealed for 5 days at 800°C. For powdering the samples a ball mill (Vario Planetenmühle, Pulverisette 4) was used. The resulting powders were compacted in a hot press (HP W 200/250-2200-200-Ks, FCT System GmbH) by 800°C and a pressure of 4kN under an argon atmosphere followed by another annealing in sealed quartz tubes at 800°C for 1 week.

RESULTS AND DISCUSSION

The clathrate I solid solution $Ba_8Au_xS_{46-x}$

The solubility range of the ternary type-I clathrate at 800 °C was studied by XRPD and EPMA on a series of samples with nominal composition $Ba_8Au_xSi_{46-x}$ (x = 3,4,5,6). Table 1 shows a comparison of the EPMA data with the results of Rietveld refinement of the X-ray spectra. In all cases the spectra could be fully indexed in the basis of a cubic clathrate type I lattice (space group P m-3n) with minor amounts of Si. As no binary clathrate type I exists under normal pressure the ternary homogeneity region is very limited at 800°C and was found to extend from 7.4 to 11.6 at% gold. The calculated lattice parameter for the clathrate series increase linear with increasing gold content and are in good agreement with those reported by Cordier et al. (single crystal data, a = 1.0422(2) for $Ba_8Au_6Si_{40,}$ [8]) and Jaussaud et al. (single crystal data, a = 1.0414(1) nm for $Ba_8Au_{5.43}Si_{40.57}$ and a = 1.0419(1) nm for $Ba_8Au_{5.89}Si_{40.11}$, [5]) (Fig.1).

Figure 2 shows the XRPD pattern of the clathrate series with increasing gold content and the Rietveld refinement for one of them. The refinement unambiguously located the Ba atoms in the 2a (0, 0, 0) and 6c $(¼,0,½)$ sites, Au and Si atoms can be found in the 6d $(¼,½,0)$ site. The Au content was fixed from EPMA measurements. Silicon occupies the 16i (x, x, x) and 24k (0, y, z) sites. Although Cordier et al. [8] reported that Au preferentially occupies the 6c site our refinement in good agreement with the results of Jaussaud et al. [5] showed for all samples, that minor amounts of Au also occupy the 24k site. No vacancies were encountered. The sample with the lowest gold content contains beside silicon a small amount of $BaSi_2$ and the other samples contain less than 1% of a second phase. Substitution of silicon atoms by gold atoms in the crystal lattice leads to different x in the 16i (x, x, x) site and changes of the coordinates of the Si3 atoms in the 24k site (0, y, z) are observed but do not show a homogeneous dependency from the gold content. The results obtained for the clathrate I series from Rietveld refinement and EPMA are combined in table 1.

Phase equilibria in the system Ba – Au – Si for 0 to 33.3 at.% Ba

The isothermal section at 800°C is shown in figure 3. At low gold contents, clathrate I is in equilibrium with silicon and $BaSi_2$. At higher gold contents, a three-phase equilibrium between clathrate I, $BaSi_2$ and $Ba(AuSi)_2$ with the AlB_2 structure type is formed. This phase oxidizes on air. From EPMA data, a quite large homogeneity region extending from $BaAu_{0.4}Si_{1.6}$ (a = 0.4193(2) and c = 0.5032(0) nm) to $BaAuSi$ (a = 0.4305(1) and c = 0.490(1) nm) can be found. The Rietveld refinement for $BaAu_{0.9}Si_{41.1}$ (a = 0.4353(4) and c = 0.4853(0) nm) as the main phase is shown in figure 4. Besides $BaAu_{0.9}Si_{41.1}$, small amounts of $BaAu_2$ (< 2%) and even less $Ba(AuSi)_4$ (no peaks found, only EPMA information) can be found in the sample.

The lattice parameter dependency for the homogeneity region is shown in figure 5 ($\frac{c}{a} \sim 1.1$ in all cases). $BaAu_2$ (AlB_2 structure type) solves about 7.5 at% gold (EPMA) at 800°C. Further investigations will be necessary for the gold rich region at about 20 at% barium ($Ba(AuSi)_4$) and about 12at% barium (π phase). The received results from EPMA and X-ray phase analysis are summarized in fig. 6 and table 2.

Analysis of the ball-milled and hot pressed sample $Ba_8Au_{5.1}S_{40.9}$

For the characterization of the ball milled-hot pressed sample, as already mentioned, X-ray powder diffraction and EPMA for phase determination were used. The powder pattern of the sample did not show a second phase but with EPMA small amounts of $Ba(AuGe)_4$ were found (fig. 7). The results from EPMA and Rietveld refinement are listed in table3. EPMA was also used to estimate the gain size after the ball-milling hot pressing procedure as described above. The size of the maintained grains is not completely homogeneous as can be seen from figure 7 (right). To find the liquidus temperature for this sample, DTA investigations were made (fig. 8).

References

[1] C. Cros, M. Pouchard, P. Hagenmuller, *C. R. Acad. Sci. Paris* **260** (1965) 4764.
 S. Kasper, P. Hagenmuller, M. Pouchard, C. Cros, *Science* **150** (1965) 1713.
 C. Cros, M. Pouchard, P. Hagenmuller, *J. Solid State Chem.* **2** (1970) 570.
[2] H. Kawai, H. O. Horie, S. Yamanaka and M. Ishikawa, *Phys.Rev.Lett.* **74**, 1427 (1995)
[3] S.Yamanaka, E. Enishi, H. Fukuoka and M. Yasukawa, *Inorg. Cem.* **39**, 56 (2000)
[4] Rüdiger F.W. Herrmann, Katsumi Tanigaki, Tetsuji Kawaguchi, Sadanori Kuroshima , Otto Zhou *Physical Review B* **60** (1999) 19
[5] N. Jaussad, P. Gravereau, S. Pechev, B. Chevalier, M. Menetrier, P. Dordor, R. Decourt, G. Goglio, C. Cros, M. Pouchard *C. R. Chimie 8* (2005) 39
[6] J.S. Tse, T. Itaka, T.Kume and H. Shimizu, K. Parlinski, H. Fukuoka and S. Yamanaka *Phsical Review B* **72**, 155441 (2005)
[7] R.F.W. Herrmann, K. Tanigaki, S. Kuroshima, H. Suematsu *Chemical Physical Letters* **283,** 29-32 (1998) [8] Cordier and Woll, *J. Less-Common. Met.* **169**, 291

(1991)

[9] Takahashi Shinji, Yamanaka Shoji *Kotai no Hannosei Toronkai Koen Yokoshu* **12** 80-82 (2001) Takahashi Shinji, Fukuoka Hiroshi, Yamanaka Shoji, Chen X, 80-83 *Nippon Kagakkai Koen Yokoshu* **79** 268 (2001)

[10] J. Rodriguez-Carvajal, FULLPROF, Abstract of the satellite meeting on powder diffraction of the 15 congress, Int. Union of Crystallography, Talence, 127 (1990)

Tables

Table 1: results from EPMA and Rietveld refinement for $Ba_8Au_xSi_{46-x}$

nominal composition	EPMA (at%)			Accepted composition[a]	lattice parameter [nm]	Si2 in 16i (x,x,x)	Si3 in 24k (0,y,z)
	Au	Ba	Si				
$Ba_8Au_3Si_{43}$	7.4	14.2	78.4	$Ba_8Au_{4.0}Si_{42}$	1.03963(4)	0.1824(7)	0.1199(5), 0.3080(1)
$Ba_8Au_5Si_{41}$	10.0	15.6	74.4	$Ba_8Au_{5.1}Si_{40.9}$	1.04130(2)	0.1832(6)	0.1165(4), 0.3043(0)
$Ba_8Au_6Si_{40}$	11.7	15.1	73.2	$Ba_8Au_{6.1}Si_{39.9}$	1.04191(2)	0.1852(7)	0.1168(6), 0.3063(8)

[a] from Rietveld refinement

Table 2: EPMA and X-ray phase analysis data for ternary alloys (quenched from 800°C) in the system Ba-Au-Si; a, b, c, d, e and f belong to the SEM images of figure 6

nominal composition (at%)			X-ray phase analysis	structure type	lattice parameter (Å)			composition (at%)		
Au	Ba	Si			a	b	c	Au	Ba	Si
5,56	14,81	79,63	(Si)	C_diam	5,429(8)	5,429(8)	5,429(8)	0	0	100
	a)		τ1	K4Ge23-x	10,3963(0)	10,3963(0)	10,3963(0)	8,3	14,2	77,6
			BaSi2	BaSi2				1,0	29,5	69,6
33	32	35	Ba(AuSi)2	AlB2	4,353(4)	4,353(4)	4,853(0)	30,0	32,6	37,4
			Ba(AuSi)4					58,0	18,2	23,8
10	25	65	Ba(AuSi)2	AlB2	4,193(2)	4,193(2)	5,032(0)	12,7	31,3	56,1
	c)		τ1	K4Ge23-x	10,406(6)	10,406(6)	10,406(6)	8,6	14,9	76,5
			BaSi2	BaSi2				0,0	31,2	68,8
60,85	14,27	24,88	Ba(AuSi)4					57,4	17,9	24,7
	f)		τ4					63,4	11,3	25,3
56,22	20,76	23,02	Ba(AuSi)2	AlB2	4,305(1)	4,305(1)	4,901(4)	32,3	31,8	35,9
	d)		Ba(AuSi)4					59,3	19,1	21,5
			BaAu2	AlB2				62,0	30,3	7,7
22,02	23,23	54,75	τ1	K4Ge23-x	10,417(8)	10,417(8)	10,417(8)	11,5	15,7	72,9
	b)		Ba(AuSi)2	AlB2	4,237(0)	4,237(0)	4,965(3)	18,5	33,3	48,2
			Ba(AuSi)4					43,9	20,8	35,3
23,53	5,88	70,59	(Si)	C_diam	5,340(7)	5,340(7)	5,340(7)	0,0	0,0	100,0
	e)		τ4					60,0	11,4	28,6
			Ba(AuSi)4					54,5	17,1	28,4
25	15	60	τ1	K4Ge23-x				12,3	15,7	72,1
			Ba(AuSi)4					51,7	18,1	30,3

Table 3: results from EPMA and Rietveld refinement for clathrate $Ba_8Au_5Si_{41}$

nominal composition	EPMA (at%)			Accepted composition[a]	lattice parameter [nm]	Si2 in 16i (x,x,x)	Si3 in 24k (0,y,z)
$Ba_8Au_5Si_{41}$	10.0	15.6	74.4	$Ba_8Au_{5.1}Si_{40.9}$	1.04130(2)	0.1832(6)	0.1165(4), 0.3043(0)

Figures
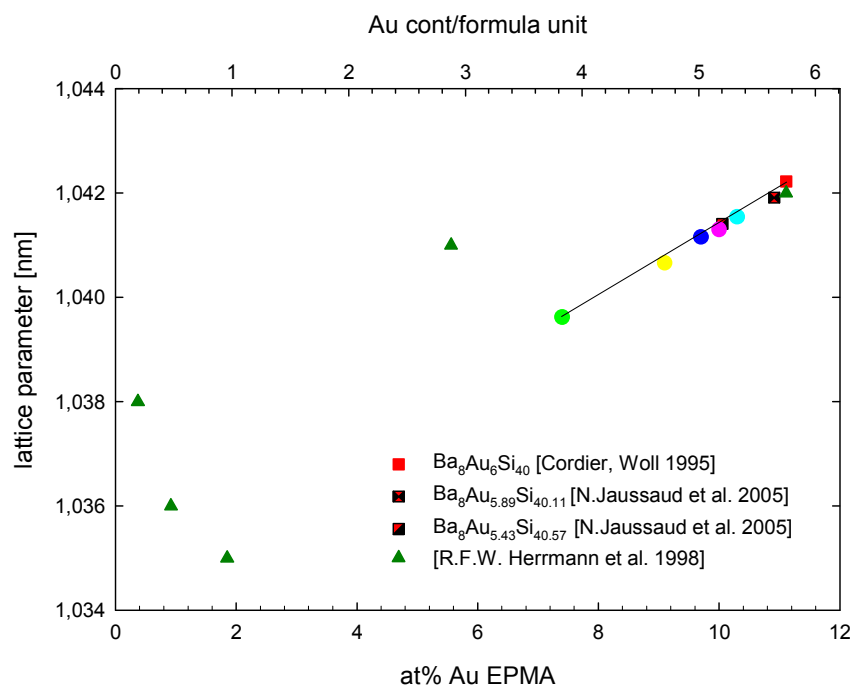
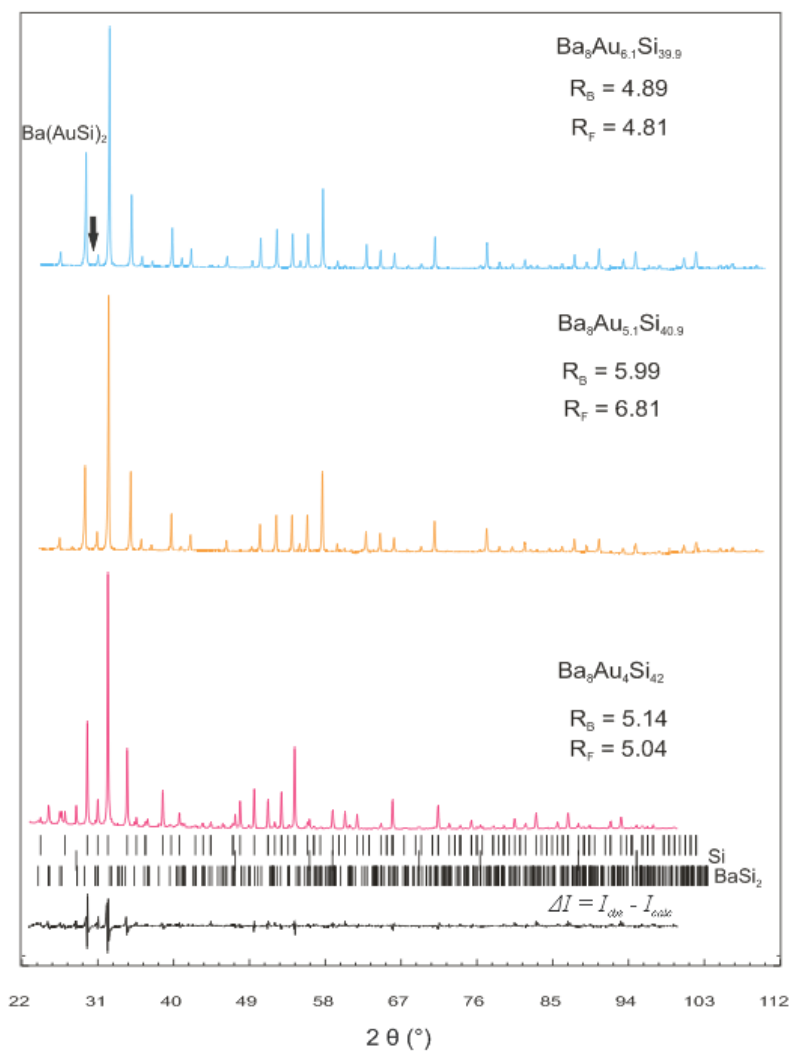Fig.1: Lattice parameters versus silver content for alloys $Ba_8Au_xSi_{46-x}$, quenched from 800°C

Fig.2: XRPD pattern and Rietveld refinement for $Ba_8Au_xSi_{46-x}$

Fig.3:

Partial isothermal section for the ternary system Ba – Au - Si at 800°C
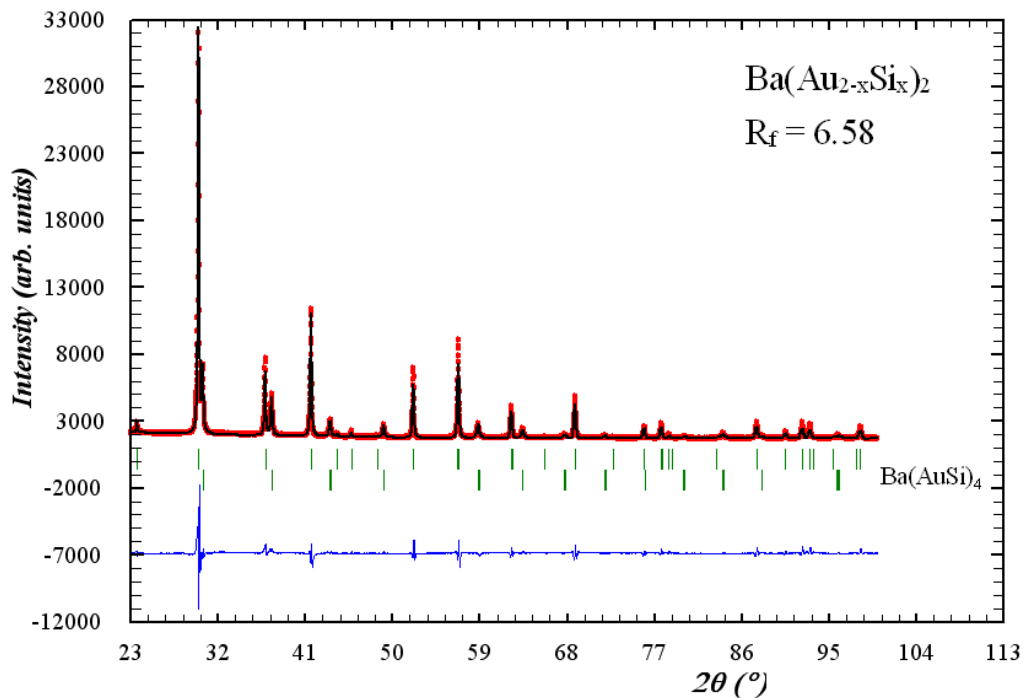
Fig 4: Rietveld refinement for Ba(Au$_{2-x}$Si$_x$)$_2$ (AlB$_2$ structure type, x = 1.1) as the main phase with less than 2% of Ba(AuSi)$_4$
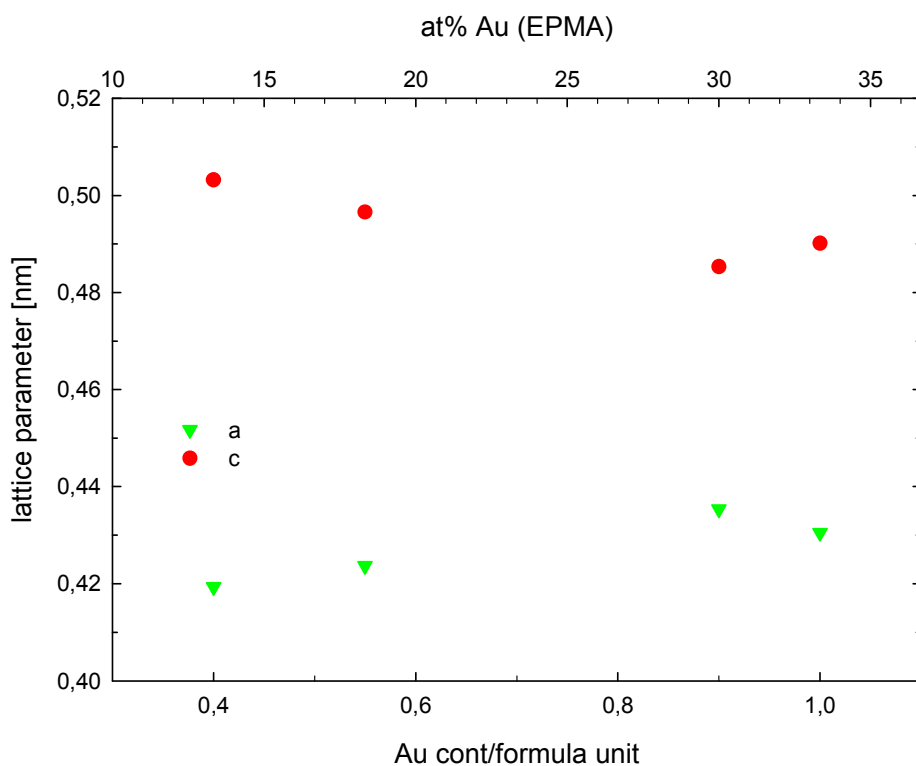
Fig. 5: Dependency of the lattice parameters from the gold content for Ba(Au$_{2-x}$Si$_x$)$_2$
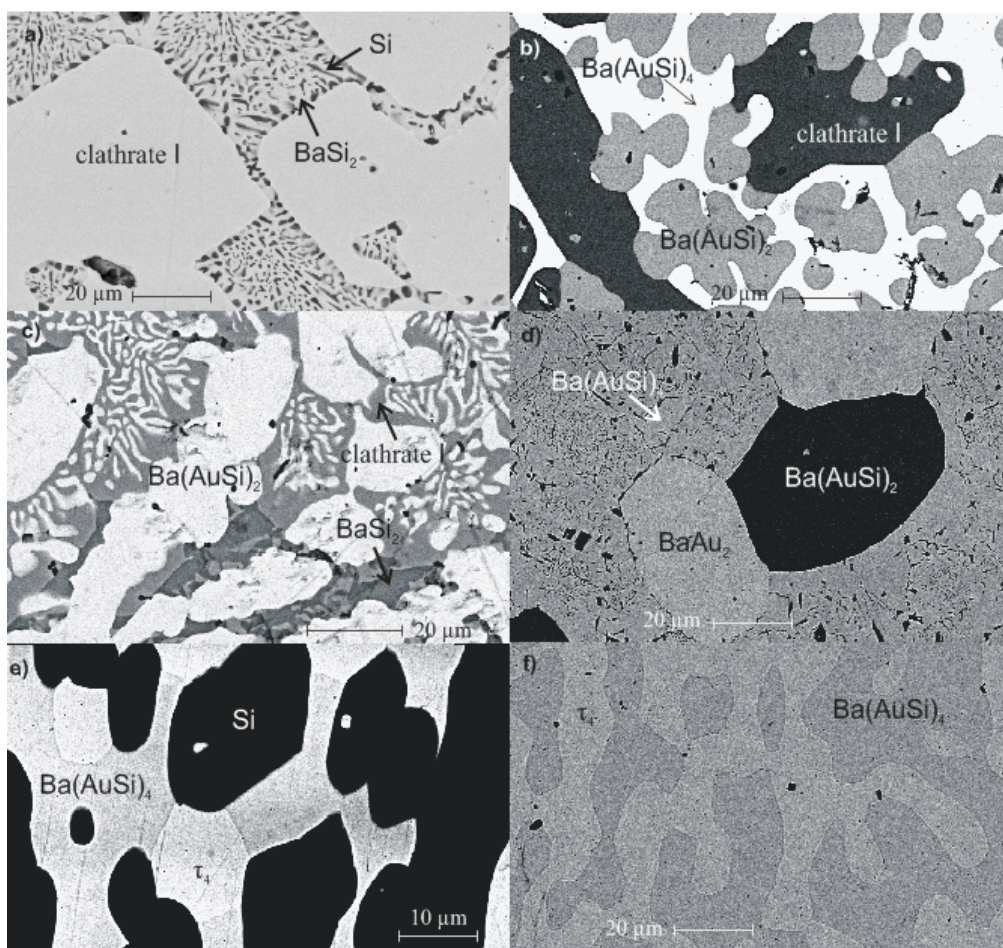
Fig. 6: SEM images of ternary or binary phase equilibria of alloys annealed at 800°C; composition of the phases a, b, c, d, e, f can be found in table 2
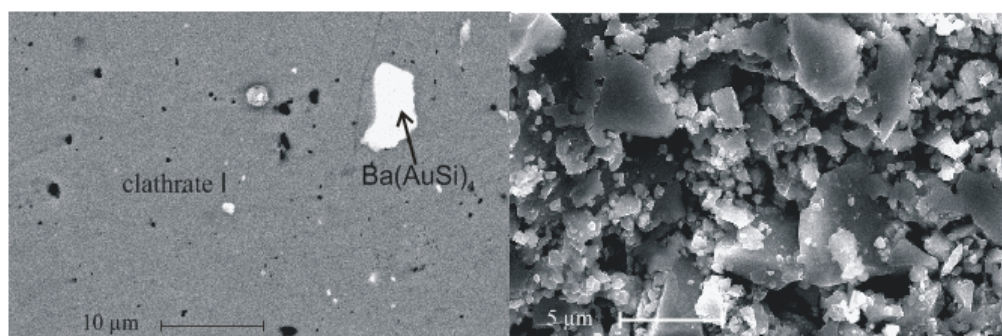
Fig. 7: SEM images of $Ba_8Au_6Ge_{40}$: phase analysis (left) and grain size (right)
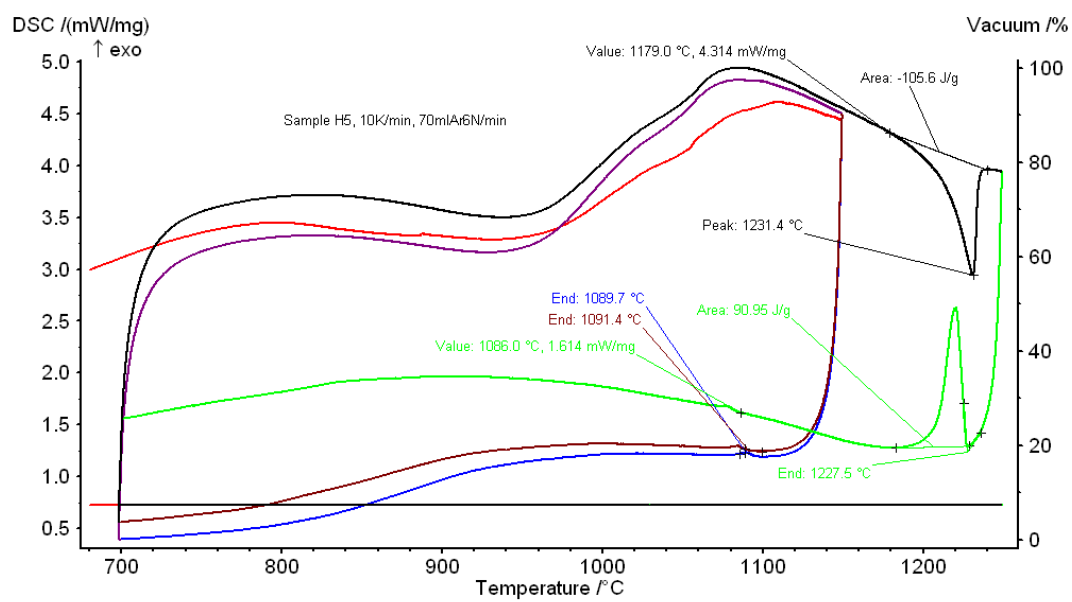
Fig.8: DSC signals from $Ba_8Au_{5.1}Su_{40.9}$

The Ba-Au-Ge system

INTRODUCTION

Although several research groups have dealt with compounds from the Au – Ba - Ge system [1,2,3,4] there is still a lack not only on the phase equilibria in the ternary system but also on the homogeneity range of the type-I clathrate solid solution $Ba_8Au_xGe_{46-x-y}\square_y$ at a defined temperature. Electrical resistivities, magnetic susceptibilities, the density of states at the Fermi level as well as the band gap have been elucidated for $Ba_8Au_6Ge_{40}$ [4], for which X-ray data seem to confirm a full atom order [1,2], without superstructure formation [6,12,13] in contrast to binary $Ba_8Ge_{43}\square_3$ with an 8-fold enlargement of the basic clathrate type I unit cell [4]. Thermoelectric properties have been studied in detail for alloys $3 \leq x \leq 6$ revealing n- and p-type behavior (*n*-type for *x*=3 to 5, *p*-type for *x*=5 to 6) [3]. Besides the clathrate type I a ternary compound $BaAu_{3.16}Ge_{0.84}$ was synthesized by melting the elements in Al_2O_3 crucibles under an argon atmosphere at about 1300°C and reported to be isotypic with the $ThCr_2Si_2$ structure type, a = 0.465 and c = 1.056 nm [5].

EXPERIMANTAL DETAILS

The samples (~1g) for the isothermal section at 800°C were prepared by arc melting from the pure elements (Ba 99.9, Au 99.9 and Ge 99.999 mass%) under an argon atmosphere. The weight loss was in all cases lower then 1-2 mass%. After arc melting they were sealed in quartz tubes under vacuum and annealed at 800°C for 1 week, were examined by X-ray diffraction techniques after which they where subdued to another annealing at 600°C for 1 month.

For the characterisation of the samples, X-ray powder diffraction (XRPD), electron probe microanalysis (EPMA) and differential thermal analysis (DTA) were used. For X-ray powder diffraction, a Guinier-Huber image plate recording system (monochromatized CuKα$_1$ radiation) was used and lattice parameters were calculated by least-square fits using Ge or Si as internal standard (a_{Ge} = 0.565791 and a_{Si} = 0.543106 nm). Rietveld refinements were made with the FULLPROF program [18]. To image the microstructure of the samples a Philips XL 30 ESEM-FEG (emission environmental scanning electron microscope) was used and the chemical composition was determined with electron probe microanalysis (EDX detector) using a Buehler Simplimett 3 and JSM 6400 SEM equipment. Differential thermal analysis was carried out in a STA 409 Netzsch differential scanning calorimeter with a heating rate of 10 K/min (5, 1, 0.1 K/min if necessary) in Y_2O_3 protective coated Al_2O_3 crucibles under an argon stream (6N, 70 ml/min). One sample of about 1 cm³ with nominal composition $Ba_8Au_6Ge_{40}$ was prepared in a different way to reach a relative density (ρ/ρ_X) higher than 96% for physical property measurements (thermopower,

resistivity and thermal conductivity). For this sample 5 alloys of 1-2g were prepared by argon arc melting the pure elements. After arc-melting they were sealed under vacuum into quartz tubes, remelted at 900°C for ~2 hours, and finally annealed for 5 days at 800°C. Powders - obtained from these alloys via ball milling in a Vario Planetenmühle (Pulverisette 4) - were then compacted in a hot press (HP W 200/250-2200-200-Ks, FCT System GmbH) at 700°C and a pressure of 4 kN under an argon atmosphere followed by another annealing in sealed quartz tubes at 800°C for 5 days.

RESULTS AND DISCUSSION

The clathrate type I solid solution $Ba_8Au_xGe_{43-x-y}\square_y$ at 800°C

The solubility range of the ternary type-I clathrate was studied by XRPD and EPMA on a series of samples with nominal composition $Ba_8Au_xGe_{46-x}$ (x = 1,2,3,4,5,6,8). Table 1 shows a comparison of the EPMA data with the results of Rietveld refinement of the X-ray spectra. In all cases the spectra could be fully indexed on the basis of a cubic clathrate type I lattice with minor amounts of Ge (< 2.2%). Starting from binary $Ba_8Ge_{43}\square_3$ the maximal solubility at 800°C for gold was found to be ~ 6.3 atoms per formula unit (11.6 to 12.2 at%) (Fig.1). The lattice parameters show a linear increase with increasing gold content with some small positive deviation at higher gold contents. Samples close to the solubility limit, show only slightly different lattice parameters which are close to that reported by Cordier and Woll for a single crystal of stoichiometric $Ba_8Au_6Ge_{40}$ (melted at 1300°C and cooled at 100K/hr; a = 1.07987(7) nm) [1]. Table 1 shows a comparison of the EPMA data with the results of Rietveld refinement of the X-ray spectra. The decreasing Ba-content with increasing gold contentis related to the amount of vacancies in the crystal lattice $Ba_8Au_xGe_{46-x-y}\square_y$. Assuming fully occupied Ba sites in the clathrate lattice (sites 2a and 6c in space group Pm3n), the vacancy concentrations calculated from EPMA, disagree only slightly with the amount of vacancies obtained from Rietveld refinement. The amount of vacancies does not decrease linearly with the increasing gold content but all voids vanished at a composition of 6 atoms of gold per unit cell (Fig. 2). In addition to the experimental data, there are two boundary models drawn in figure 2. Model A assumes, that there is only a substitution of germanium atoms and no filling of vacancies $Ba_8Au_xGe_{43-x}\square_3$. The second model delineates first all the vacancies and after that the Ge / Au exchange occurs. The experimental data are in between these two models. This means that filling vacancies and substitution of Ge atoms takes place simultaneously. This is in quite good agreement with the results reported for other ternary clathrates such as Ba-Zn-Ge [7], Ba-Pt-Ge [8], BaPdGe [10], BaCdGe [11].

Figure 3 shows the XRPD pattern of samples with increasing gold content and the Rietveld refinement for one of them. No extra reflections for a larger unit cell a' = 2a as reported [4,12,13] for

binary $Ba_8Ge_{43}\square_3$ were observed. The refinement in all cases confirmed the Ba atoms in the sites 2a $(0, 0, 0)$ and 6c $(\frac{1}{4},0,\frac{1}{2})$, Ge atoms in the sites 16i (x, x, x) and 24k (0, y, z), whereas Au, Ge atoms and vacancies can be found in the 6d $(\frac{1}{4},\frac{1}{2},0)$. Because refinement of occupancies for three species in one site is not reliable, the Au content was fixed from EPMA measurements. Cordier et al. [1] as well as Johnsen et al. [2] reported that Au preferentially occupies the 6c site. The refinement for the samples with highest gold content (6 gold atoms per formula unit) showed, that a small amount of gold also enters the 24k site in agreement with the findings of Johnsen et al. [2]. In the x-ray powder spectra the increasing gold content can be seen in the intensity ratio of 3 peaks indexed as (222), (320) and (321). The positional parameters y and z of the 24k site, received from Rietveld refinement, decrease with increasing gold content (Fig. 4). Substitution of germanium atoms by gold atoms in the crystal lattice does not lead to largely different x in the site 16i (x, x, x) whilst changes of the coordinates of the Ge3 atoms in the site 24k (0, y, z) are observed. The positional parameter y and z of the 24k site, decrease with increasing gold content (Fig. 5).

Phase equilibria in the ternary system Ba – Au – Ge for 0 to 33.3 at.% Ba

The isothermal section at 800°C for the germanium and gold rich part is shown in figure 5. Type-I clathrate is in equilibrium with clathrate type-IX (Ba_6Ge_{25} structure type). The maximum solubility of gold in clathrate IX at 800°C is 2.7 at% (a = 1.4559(8) nm). Alloys containing moisture sensitive $BaGe_2$ ($BaSi_2$ structure type), quickly decompose on air. At the solubility limit of gold in clathrate I, a three phase equilibrium exists between the clathrate $BaGe_2$ and. At low gold contents, (24.2 at% Au, 20.4 at% Ba and 55.4 at% Ge from EPMA) the Rietveld refinement for $Ba(AuGe)_4$ indicates most probably the $BaNiSn_3$ structure type (a = 0.4650(4) and c = 1.033(3) nm) (fig. 6). Samples with higher gold content show a different powder pattern indicating a different structure type (fig. 7) but in any case no correspondence to the $ThCr_2Si_2$ structure type was found as reported by N. May and H. Schäfer [5] for $BaAu_{3.16}Ge_{0.84}$. The secondary phase in the other 2 samples shown in fig. 8, is $Ba(AuGe)_2$ with the AlB_2 structure type. In the ternary Ba – Au – Ge system $Ba(AuGe)_2$ (AlB_2 structure type) exists at 800 °C and a second phase extending from the binary $BaAu_2$ also has this structure type. $Ba(AuGe)_2$ shows a quite large homogeneity range from $BaAu_{0.5}Ge_{1.5}$ (a = 0.4381(0) and c = 0.4929(7) nm) to $BaAu_{0.9}Ge_{1.1}$ (a = 0.4656(8) and c = 0.497(9) nm) with $\frac{c}{a} \sim 1.1$ in all cases. The Rietveld refinement for the sample with low gold content and a small content (9%) of $Ba(AuGe)_4$ as a second phase is shown in figure 8. The second phase with AlB_2 structure type extends at 800°C from binary $BaAu_2$ (a = 0.4804 and c = 0.4119 nm) [14] to a solubility limit of about 5.4 at % (from EPMA, $BaAu_{1.8}Ge_{0.2}$ with a = 0.4983(4), c = 0.4346(3) nm and $\frac{c}{a} \sim 0.9$). $BaAu_{1.8}Ge_{0.2}$ and $BaAu_{1.8}Ge_{0.2}$ oxidize on air as can be seen from the microstructure image in figure 9. Another ternary phase (τ) with hitherto unknown crystal structure exists in the gold rich part of

the phase diagram. From electron probe micro- analysis it contains about 60 at% gold, 12 at% barium and 28 at% germanium. Results from EPMA measurements and X-ray phase analysis are summarized in table 2.

Analysis of the ball-milled and hot pressed sample $Ba_8Au_6Ge_{40}$

For the characterization of the ball milled and hot pressed sample, as already mentioned, X-ray powder diffraction, EPMA for phase and grain size determination as well as DTA were used. The Rietveld refinement of the powder pattern shows small amounts (~2.5%) of $Ba(AuGe)_4$ as a second phase. This is in good agreement with the results from EPMA (fig. 10). The results from EPMA and Rietveld refinement are summed in table 3.

EPMA was also used to estimate the gain size after the ball-milling and hot pressing procedure as described above. The maintained grains are not completely homogeneous as can be seen from figure 11 (right). To find the liquidus temperature for this sample, DTA investigations were made (fig. 12) revealing a liquidus temperature at about 926 °C and a solidus temperature at about 885°C.

References

[1] G. Cordier, P. Woll *J. Less-Common. Met.* **169** (1991) 291
[2] S. Johnsen, B. Thomsen, M. Christensen, G.K.H. Madsen, M. Nygren, B. Inversen (2007) ICT
[3] H. Anno, M. Hokazone, H. Takakura K. Matsubara (2005) ICT
[4] Rüdiger F.W. Herrmann, Katsumi Tanigaki, Tetsuji Kawaguchi, Sadanori Kuroshima , Otto Zhou *Physical Review B* **60** (1999) 19
[5] N. May, H. Schäfer *Z. Naturf.* **27B** (1972) 864
[6] W. Carrillo-Cabrera, S. Budnyk, Y. Prots, and Y. Grin *Z. Anorg. Allg. Chem*. **630** (2004) 7226
[7] N. Melnychenko-Koblyuk, A. Grytsiv, L. Fornasari, H. Kaldarar, H. Michor, F. Röhrbacher, M. Koza. E. Royanian, E. Bauer, P. Rogl, M. Rotter, H. Schmid, F. Marabelli, A. Devishvili, M. Doerr, G. Giester *J.Phys.: Condens. Matter* **19** (2007) 216223
[8] N. Melnychenko-Koblyuk, A. Grytsiv, G. Giester, E. Bauer, P. Rogl, M. Rotter, L. Lackner, L. Fornasari, F. Marabelli *Phys. Rev. B* **76 (**2007) 195124
[10] N. Melnychenko-Koblyuk, A. Grytsiv, G. Giester, E. Bauer, P. Rogl, M. Rotter, G. Durand, H. Kaldarar, R. Lackner, H. Michor, E. Royanian M. Koza *Phys. Rev. B* **76 (**2007) 144118
[11] N. Melnychenko-Koblyuk, A. Grytsiv G. Giester, St. Berger, H. Kaldarar, H. Michor, F. Röhrbacher, E. Royanian, E. Bauer, P. Rogl, M. Rotter, H. Schmid, *J.Phys.: Condens. Matter* **19** (2007) 046203
[12] W. Carrillo-Cabrera, J. Curda, K. Peters, S. Paschen, M. Baenitz, Yu. Grin, H.G. von Schnering *Z. Kristallogr*. *NCS* **215** (2000) 321
[13] N.L. Okamoto, M.W. Oh, T. Nishii, K. Tanaka, H. Inui *J. Appl. Phys.* **99** (2006) 033513
[14] G. Bruzzone and G.B. Bonino, Atti della Accademia Nazionale dei Lincei, Classe di Scienze Fisiche, Matematiche e Naturali, Rendiconti (1970) 48, 235-241

Tables

Table 1: Composition and crystallographic data from EPMA and Rietveld refinement for the clathrate type I solid solution $Ba_8Au_xGe_{43-x-y}\square_y$

nominal composition	EPMA (at%)			Accepted composition[a]	lattice parameter nm	Ge2 in 16i (x,x,x)	Ge3 in 24k (0,y,z)
	Ba	Au	Ge				
$Ba_8Ag_2Ge_{44}$	15.6	4.5	79.9	$Ba_8Au_{2.2}Ge_{41.4}\square_{2.4}$	1.07081(2)	0.1830(0)	y=0.1194(2) z=0.3175(5)
$Ba_8Ag_4Ge_{42}$	15.1	8.4	76.5	$BaAu_{4.4}Ge_{40.3}\square_{1.3}$	1.07726(2)	0.1835(7)	0.1184(2), 0.3107(8)
$Ba_8Ag_6Ge_{40}$	15.0	11.3	73.7	$BaAu_6Ge_{40}$	1.07969(1)	0.1836(4)	0.1121(3), 0.3196(0)

[a] from Rietveld refinement

Table 2: X-ray phase analysis, lattice parameters and phase composition from EPMA for Ba-Au-Ge alloys annealed at 800°C

nominal composition (at%)			X-ray phase analysis	structure type	lattice parameter (Å)			composition EPMA (EDX) (at%)		
Au	Ba	Ge			a	b	c	Au	Ba	Ge
1.85	14.81	83.34	(Ge)	C_dia	10,682(0)	10,682(0)	10,682(0)	0	0	100
			w	K_xGe_{23-x}	9.649(1)	9.649(1)	9.649(1)	2.5	14.2	83.1
5.56	14.81	79.63	cIX	IIa(AuGe)_4	14,559(8)	14,559(8)	14,559(8)	2.2	18.0	79.8
		b)	xI	K_xGe_{23-x}	10,755(0)	10,755(0)	10,755(0)	7.2	14.7	78.1
6.10	73.41	80.7	IIa(AuGe)_4	IIaNiSn_2				73.4	20.5	17.1
	a)		xI	K_xGe_{23-x}	10,795(0)	10,795(0)	10,795(0)	11.3	15.4	73.4
			BaGe_2	BaSi_2	9,07(18)	6,80(86)	11,63(63)	0.3	33.0	66.7
17.25	30.89	51.86	Ba_2AuGe_3	BaNiSn_3	4.647(2)	4.647(1)	10.667(0)	73.1	18.3	18.6
			IIa(AuGe)_4	AlB_2	4,647(5)	4,647(5)	4,929(7)	16.2	30.0	53.7
15	33	34	Ba_2AuGe_3					47.1	20.0	32.9
	c)		IIa(AuGe)_4	AlB_2	4,649(0)	4,649(0)	4,97(96)	50.7	32.1	16.3
			Ba_2Au_2	AlB_2	4,983(4)	4,983(4)	4,349(3)	61.4	33.0	5.4
40.3	21.5	38.2	Ba_2AuGe_3	AlB_2	4,429(1)	4,429(4)	4,396(67)	74.6	32.2	41.2
			Ba_2AuGe_3	ThCr_2Si_2				42.6	20.4	37.0
48.6	17.01	34.32	Ba_2AuGe_3					47.7	19.6	31.0
	d)		(Ge)	C_dia				0.0	0.0	100.0
			c					67.8	11.8	75.4
62.48	20.95	16.57	IIa(AuGe)_4					60.24	19.16	20.6
	e)		Ba_2Au_2	AlB_2	4,807(1)	4,807(1)	4,176(1)	66.17	32.31	1.76
21	60	19	IIa(AuGe)_4	IIaNiSn_2	4,650(4)	4,650(4)	10.33(3)	60.2	19.2	20.6
			w	K_xGe_{23-x}	10.795(7)	10.795(2)	10.795(2)	11.1	15.1	73.8

Table 3: results from EPMA and Rietveld refinement

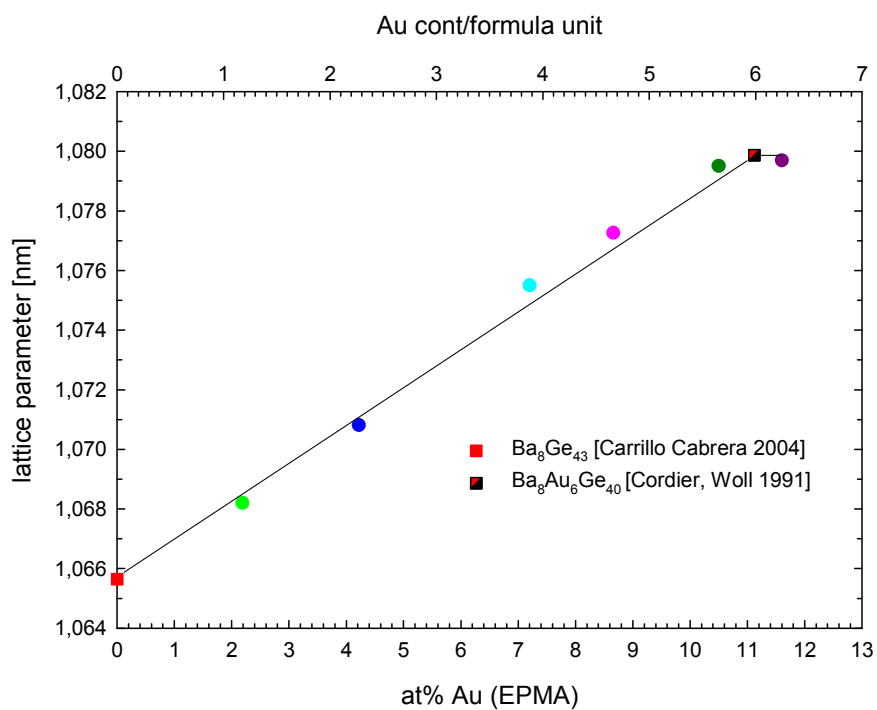| nominal composition	EPMA (at%)			Accepted composition[a]	lattice parameter [nm]
	Ba	Au	Ge		
$Ba_8Au_6Ge_{40}$	15.0	11.3	73.7	$Ba_8Au_6Ge_{40}$	1.07969(1)

[a] from Rietveld refinement

Figures

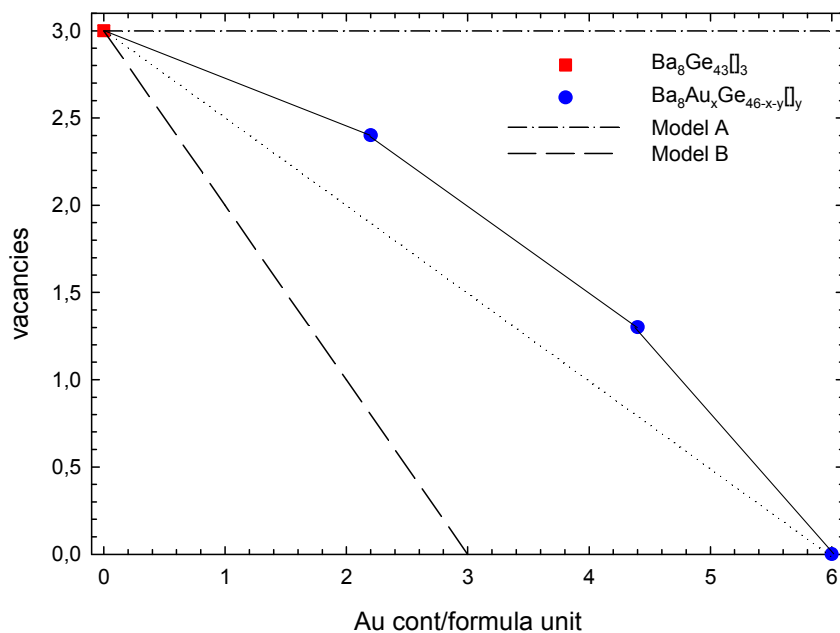Fig.1: Lattice parameters vs Au-content for the clathrate type I solid solution $Ba_8Au_xGe_{43-x-y}\square_y$

Fig. 2: Amount of vacancies vs. gold content per formula unit for the clathrate type I solid solution $Ba_8Au_xGe_{43-x-y}\square_y$
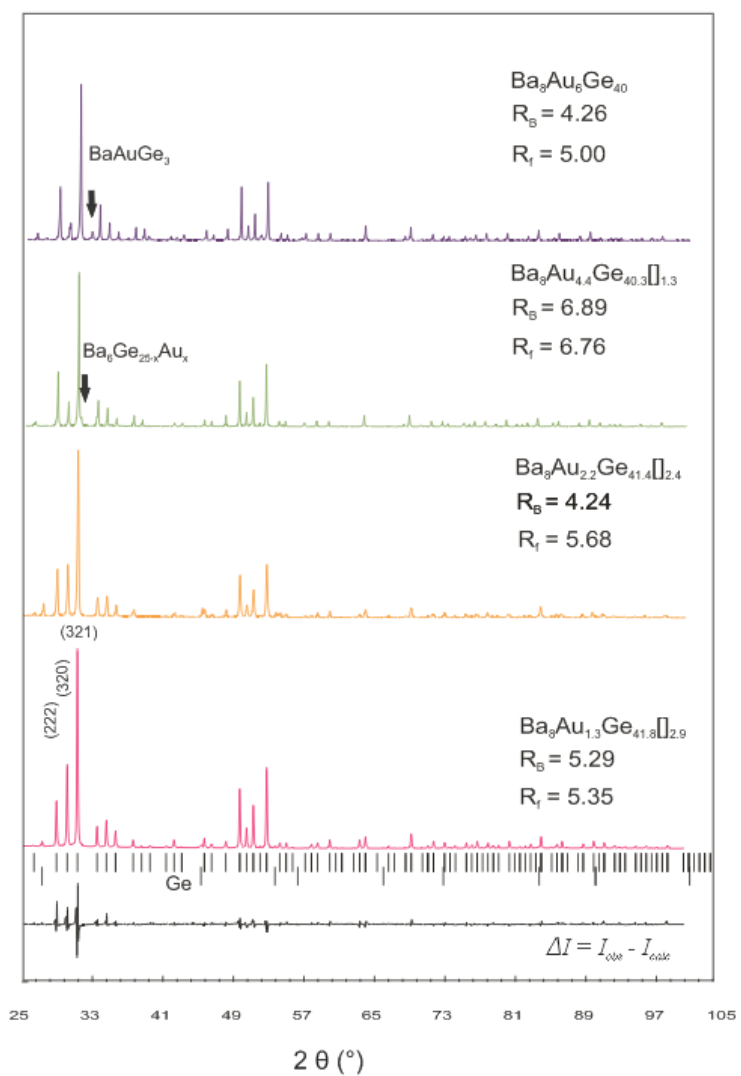
Fig. 3: XRPD pattern and Rietveld refinement for samples $Ba_8Au_xGe_{46-x-y}\square_y$ (x = 1.3, 2.2, 4.4 and 6); secondary phases are indicated by arrows.
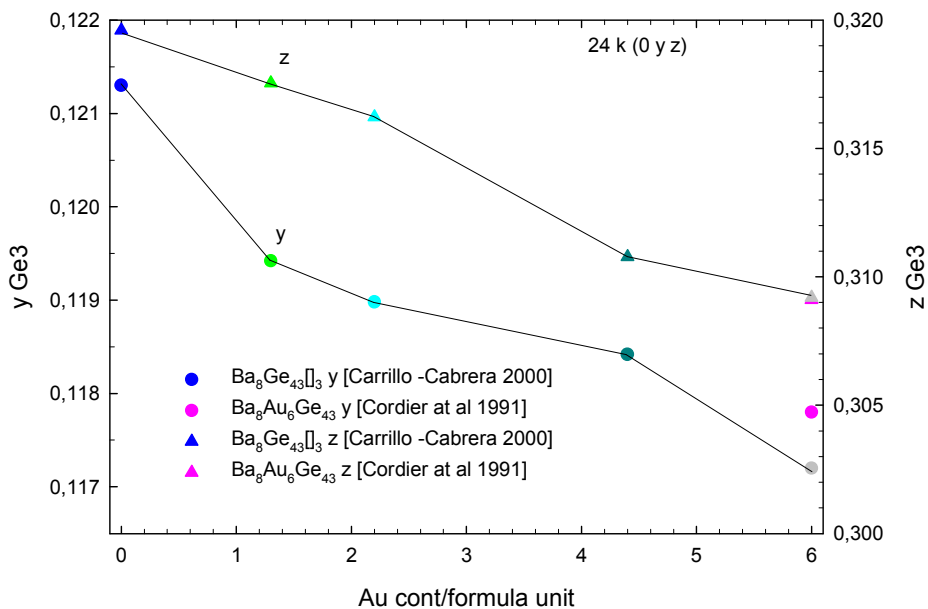
Fig. 4: Au content per formula unit in $Ba_8Au_xGe_{46-x-y}\square_y$ vs. compositional parameters y and z for the Ge3 site (24k (0, y, z))
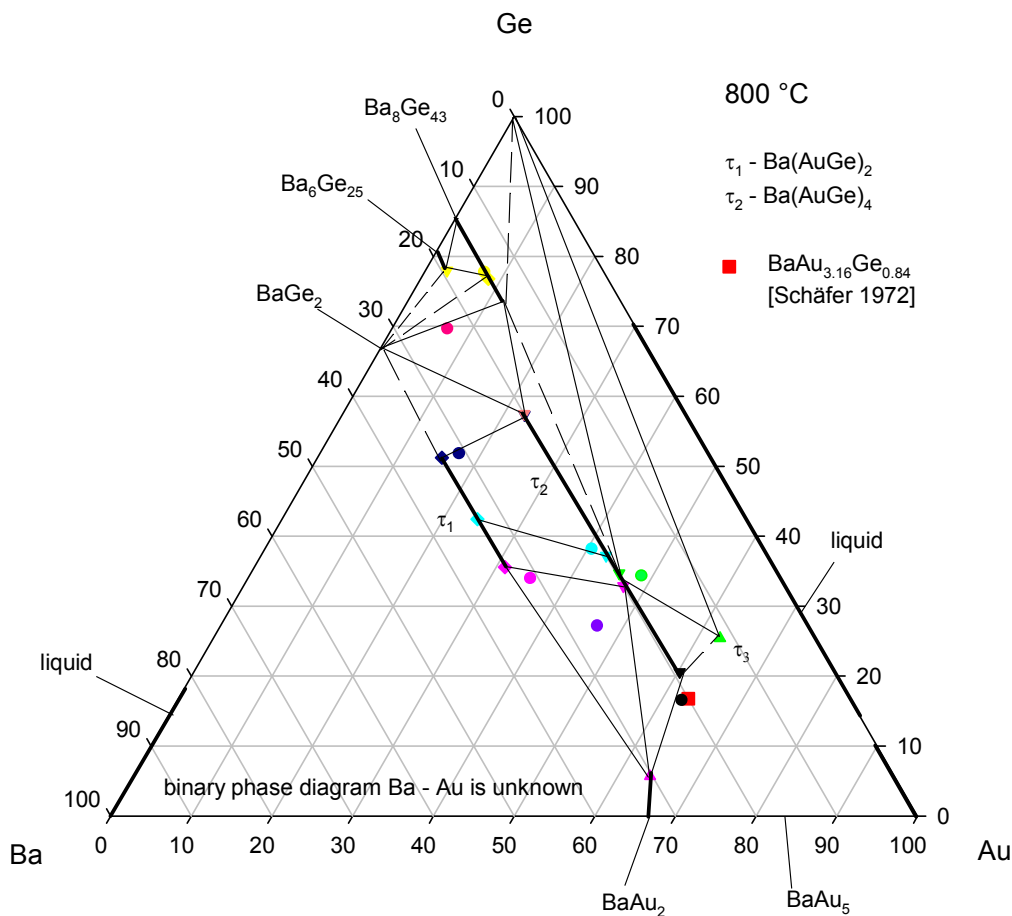
Fig. 5: partial isothermal section at 800°C of the ternary Ba – Au - Ge
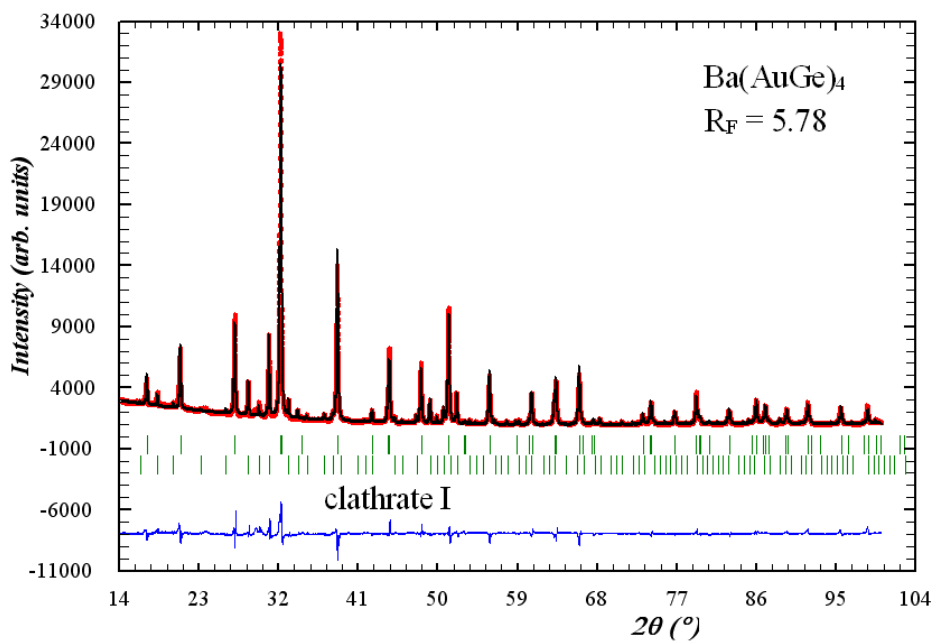
Fig. 6: Rietveld refinement for Ba(AuSi)$_4$ (BaNiSn$_3$ structure type) and clathrate I (<18%)
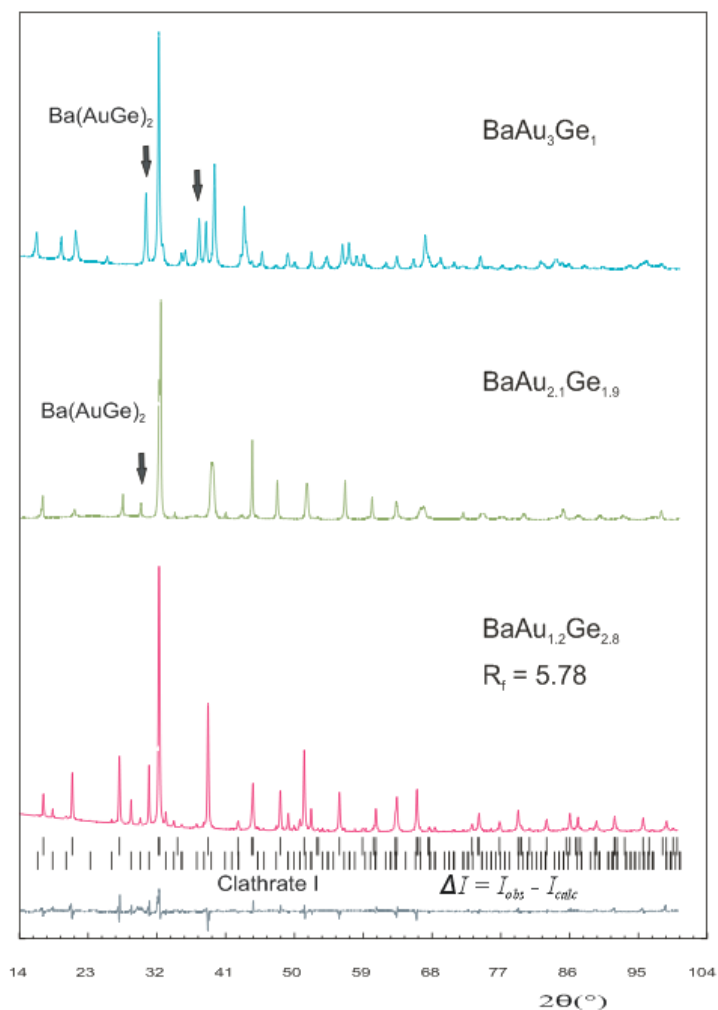
Fig. 7: powder pattern for 3 samples of Ba(AuGe)$_4$ as the main phase. The Rietveld refinement is shown for the sample

with the lowest gold content containing about 18% clathrate I as secondary phase
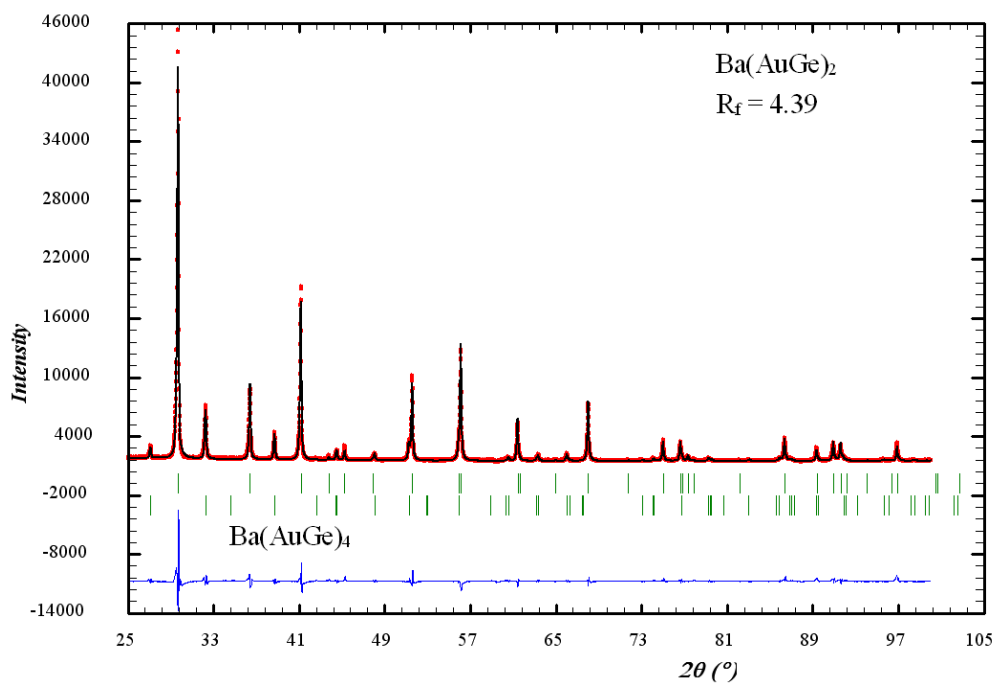
Fig. 8: Rietveld refinement for BaAu$_{0.5}$Ge$_{1.5}$ (EPMA) with AlB$_2$ structure type and Ba(AuGe)$_4$ (BaNiSn$_3$ structure type)
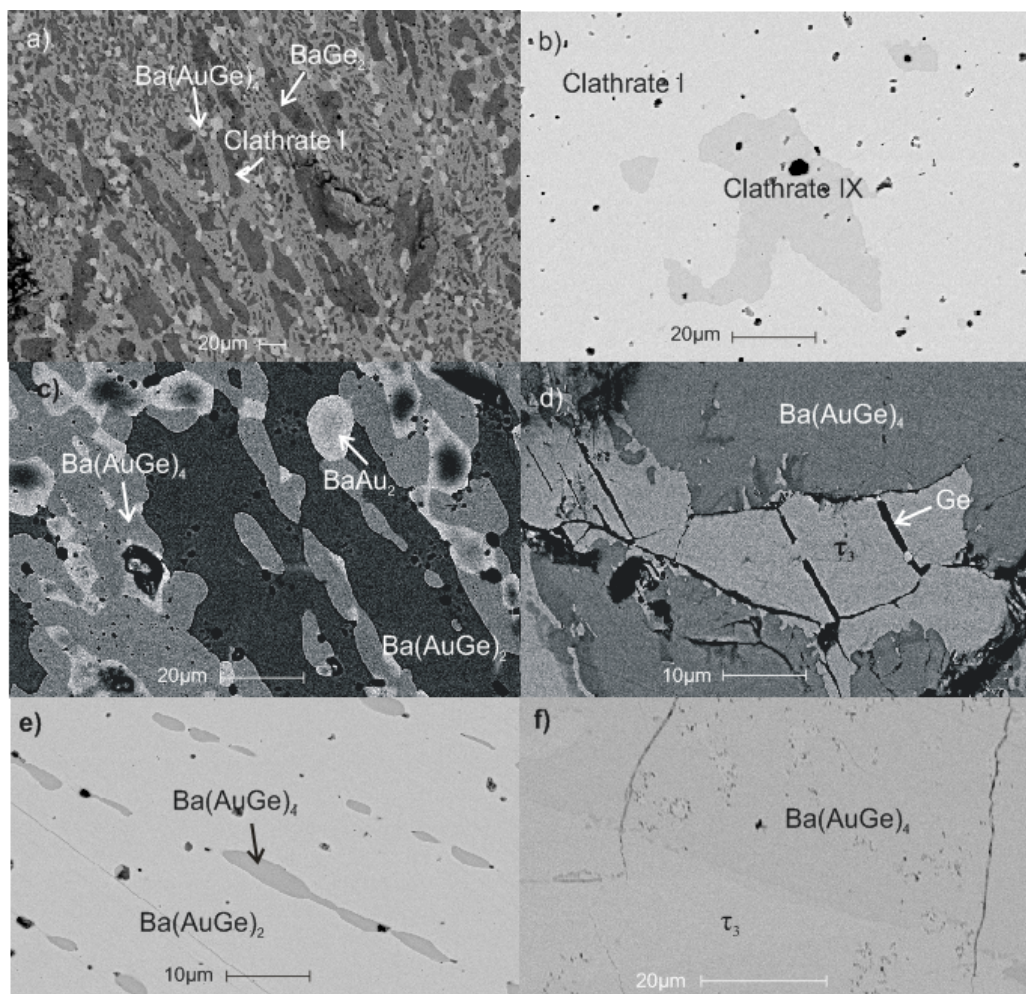
Fig. 9: microstructures of several Ba – Au – Ge alloys (annealed at 800°C) revealing binary or ternary phase equilibria; the composition of the phases in a, b ,c ,d, e, f can be found in table 2
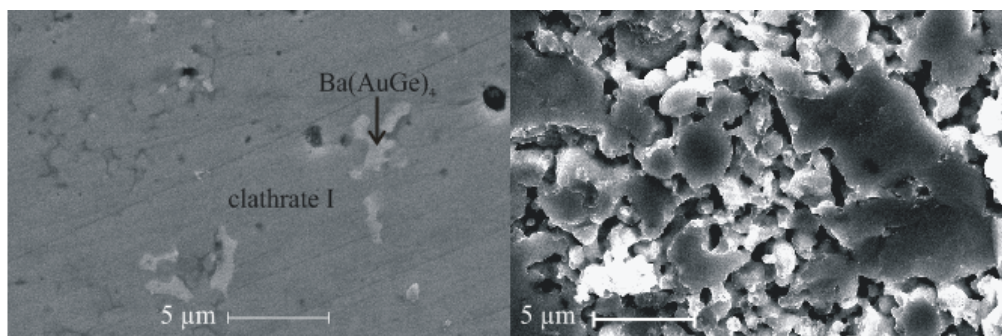
Fig. 10: SEM images of $Ba_8Au_6Ge_{40}$: phase analysis (left) and grain size (right)
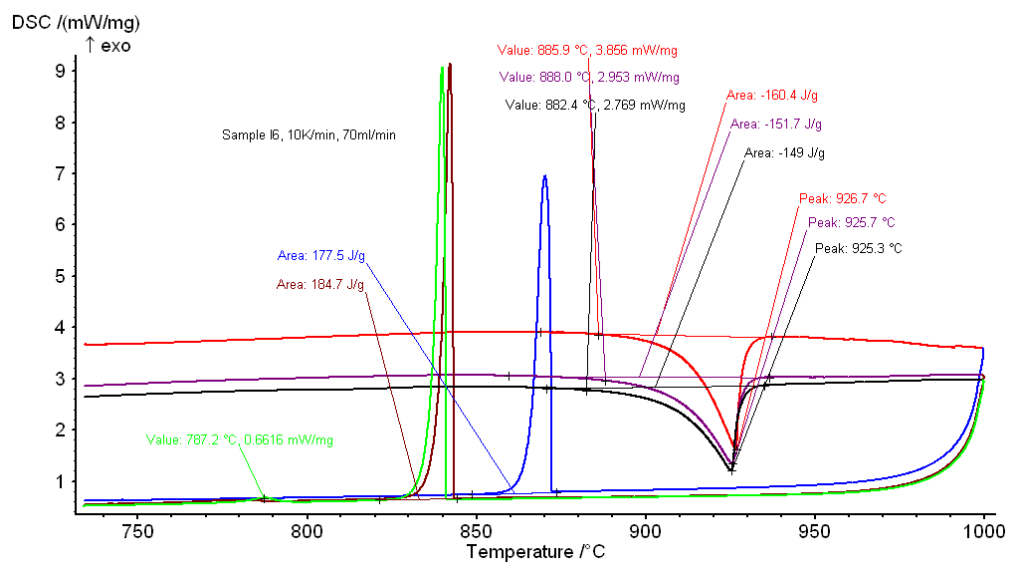
Fig. 12: DSC signals for $Ba_8Au_6Ge_{40}$

Physical properties of the clathrates $Ba_8Au_6Ge_{40}$, $Ba_8Au_{5.1}Si_{40.9}$ and $Ba_8Ag_5Si_{41}$

Introduction

A thermoelectric material is best characterized by its figure of merit (ZT).

$$ZT = \frac{S^2 T}{\rho \lambda} \qquad\qquad (1)$$

From this equation can be seen, that a good thermoelectric material should provide large thermopower in addition to high electrical conductivity (ρ = electrical resistivity) and low thermal conductivity. It has been shown, that n- and p-type materials can be produced through substitution of silicon or germanium framework atoms in $M_x(Si,Ge)_{46}$ (M = alkali or alkaline-earth) with noble metals (Au) [1,2]. Several research groups have already investigated some of the Ag, Au containing Si- and Ge-based clathrates type one but mostly at temperatures below room temperature. Jaussaud et al. measured low temperature (<300 K) resistivity and thermopower of $Ba_8Au_{5.43}Si_{40.57}$ (n-type) and $Ba_8Au_{5.89}Si_{40.11}$ (p-type) [2]. Thermoelectric properties for the series $Ba_8Au_xGe_{46-x}$ with x = 3-6 above room temperature were investigated by Anno et al. [1]. The magnetic susceptibility, low temperature electrical resistivity (< 300 K), the density of states at the Fermi level and the band gap were determined by Hermann et al. [3] for Ba_8Ge_{43}, $Ba_8Au_6Si_{40}$ and $Ba_8Au_6Ge_{40}$. Johnsen et al. [4] reported Hall resistivity, electrical resistivity and thermopower data for $Ba_8Au_6Ge_{40}$ and $Ba_8Ag_6Ge_{40}$. The investigations performed in this work, include thermopower measurements in the temperature range between 4.2 and 900 K, electrical resistivity measurements in the same temperature range and thermal conductivity measurements between 6 and ~ 300 K for three selected samples: $Ba_8Ag_5Si_{41}$, $Ba_8Au_{5.1}Si_{40.9}$ and $Ba_8Au_6Ge_{40}$.

Experimental Detail

For each sample of about 1 cm³, 5 smaller samples with a weight of 1-2g were prepared by arc melting from the pure elements under an argon atmosphere. After arc melting they were sealed under vacuum into quartz tubes and annealed for 5 days at 800°C. For powdering the samples a ball mill (Vario Planetenmühle, Pulverisette 4) was used. The resulting powders were compacted in a hot press (HP W 200/250-2200-200-Ks, FCT System GmbH) by 800°C (Si clathrates) or 700°C (Ge clathrates) and a pressure of 4kN under an argon atmosphere followed by another annealing in sealed quartz tubes at 800°C for 1 week.

For the characterisation of the samples, X-ray powder diffraction (XRPD), electron probe microanalysis (EPMA) and differential thermal analysis (DTA) were used (results are already

described in other chapters).

The samples were cut into cuboids (~1.5x1.5x8 mm³) with a diamond saw for resistivity, thermopower and thermal conductivity measurements. Low temperature electrical resistivity measurements (from 4.2 to 300K) were carried out in a conventional ^{4}He cryostat using a dc four-point technique. For thermopower measurements in the same low temperature range, a four-point technique using a differential method and seesaw heating was employed.

$$S_x = S_{Ch} - \frac{V_{Ch}}{V_{Ch} - V_{Co}}(S_{Ch} - S_{Co})$$

(1)

With equation (1) the absolute thermopower (S_x) can be calculated using the absolute thermopower of chromel (S_{Ch}) and constantan (S_{Co}) and the voltages along the chromel and constantan circuit (V_{Ch} and V_{Co}). The sample is glued at both ends to the heater (strain gauge) panels with G.E.-varnish and the chromel/constantan thermocouples are contacted with conduction silver because soldering is not possible for most clathrates. For temperature measurements, a Pt100 sensor and below 30 K a Ge resistive sensor was used.

Measurements of thermopower and resistivity at high temperatures (300 – 1000 K) were carried out simultaneously on an ULVAC equipment (ZEM-3, Japan). For electrical resistivity a four point technique is used whereas thermopower is measured with a statistic dc method.

The thermal conductivity was also measured in the low temperature range between 5 and 290 K with a steady state heat flow method.

Results and discussion

Temperature dependent electrical resistivity

The temperature dependency of the electrical resistivity for the 3 samples is summed in Fig.1 (nominal composition). For $Ba_8Au_6Ge_{40}$ and $Ba_8Ag_5Si_{41}$ a metal-like behaviour and a much lower electrical resistivity than for the sample with gold and silicon were found. A broad maximum at high temperatures was also observed for $Ba_8Au_{5.1}Si_{40.9}$.

All samples show a minimum at low temperatures that is most distinct for the sample with gold and silicon. For a theoretical description of the experimental results, the Bloch-Grüneisen model and the 2-band model with Mott-Jones term was used. The Bloch-Grüneisen model describes the temperature dependency of the electrical resistivity for metals. In case of metals, at temperatures above room temperature, the resistivity increases linear with the temperature. Because of changing electron-phonon interactions at low temperatures, the resistivity dependency changes and is proportional to T^5. At very low temperatures (T→ 0K), the residual resistance is only dependent on

defects in the material. The temperature dependent resistivity is according to Matthiessen's formula:

$$\rho(T) = \rho_0 + \rho_{ph}(T) \tag{2}$$

which refers to the Bloch-Grüneisen part :

$$\rho_{ph} = R\left(\frac{T}{\theta_D}\right)^5 \int_0^{\frac{\theta_D}{T}} \frac{z^5}{(e^z - 1)(1 - e^{-z})} \tag{3}$$

An advancement of the Bloch-Grüneisen model is the addition of a temperature dependent charge carrier density n(T) and a term proportional to T^3 while using the Bloch-Grüneisen formula for ρ_{ph}, leading to the 2-band model with Mott-Jones term[5,6]:

$$\rho(T) = \frac{\rho_0 n_0 + \rho_{ph}}{n(T)} + \frac{AT^3}{n(T)} \tag{4}$$

The least square fits have been carried out with the *Table Curve 2D Version 5.01*

The high temperature maximum of $Ba_8Au_5Si_{41}$ can be described with the 2-band model with Mott-Jones term (Fig.2) and also the minimum at low temperatures is described quite well. For fit parameters see Table 1. The temperature dependency of the resistivity of the silver sample is quite different. Over the whole temperature range it shows a metal-like behaviour. For $Ba_8Ag_5Si_{40}$, the experimental can be fitted with the Bloch-Grüneisen model and with the 2-band model with Mott-Jones term (Fig. 3). For fit parameters see Table 1. The lowest electrical resistivity shows $Ba_8Au_6Ge_{40}$ (Fig.4) and it seems to have also a maximum at high temperatures. The used user defined functions and explanations of the fitting parameters are taken from [8].

Temperature dependent thermopower

The experimental results of the temperature dependent thermopower are shown in Fig.6. $Ba_8Au_{5.1}Si_{40.9}$ and $Ba_8Ag_5Si_{41}$ show n-type behaviour with the highest values for the thermopower reached at about 560 K (S = -98 µV/K) for the gold sample and at about 800 K (S = -75µV/K) for the silver sample. $Ba_8Au_6Ge_{40}$ shows p-type behaviour in agreement with literature data [1] with a maximum thermopower at about 880 K (S = 123 µV/K).

From the almost linear increase of the thermopower at temperatures below 300K,

the charge carrier density (n), can be calculated using equation 4:

$$S = \frac{\pi^2 k_B{}^2 2m_e}{|e|h^2 (3n\pi^2)^{3/2}} \cdot T \tag{5}$$

$$|e| = 1.6022 \cdot 10^{-19} \text{ [As]}$$

$$k_B = 1.3807 \cdot 10^{-23} \text{ [J/K]}$$

$$h = 1.0546 \cdot 10^{-34} \text{ [m}^2\text{s}^{-1}\text{kg]}$$

$$m_e = 9.1094 \cdot 10^{-31} \text{ [kg]}$$

$Ba_8Au_{5.1}Si_{40.9}$: $n = 2.045 \cdot 10^{21}$ [cm^{-3}]

$Ba_8Ag_5Si_{41}$: $n = 6.144 \cdot 10^{20}$ [cm^{-3}]

$Ba_8Au_6Ge_{40}$: $n = 1.2225 \cdot 10^{21}$ [cm^{-3}]

Temperature dependent thermal conductivity

The temperature dependent thermal conductivity was measured in the temperature range between 10 and about 300 K. A generally larger thermal conductivity was found for $Ba_8Ag_5Si_{41}$ (Fig.7). In this sample, a maximum at low temperatures appears, but in all cases the overall values are quite low which is usual for cage forming compounds.

For a more detailed consideration the thermal conductivity can be separated into the lattice thermal conductivity (λ_{ph}) and the electronic contribution to the thermal conductivity (λ_e):

$$\lambda = \lambda_{ph} + \lambda_e \tag{6}$$

The electronic contribution to the thermal conductivity can be calculated using the Wiedemann-Franz law:

$$\lambda_e = \frac{L_0 T}{\rho} \tag{7}$$

with the electrical resistivity (ρ) and the Lorentz number ($L_0 = 2.45*10^{-8}$ WΩ/K^2).

The lattice thermal conductivity according to Callaway [7] with a radiation loss term FT^3 can be written as:

$$\lambda_{ph} = CT^3 \int_0^{\frac{\theta_D}{T}} \frac{\tau_c x^4 e^x}{\left(e^x - 1\right)^2} dx + FT^3 \tag{8}$$

The overall relaxation time for scattering processes (τ_c) can be written as the sum of various scattering processes:

$$\tau_c^{-1} = \tau_B^{-1} + \tau_D^{-1} + \tau_u^{-1} + \tau_E^{-1} \tag{9}$$

τ_B ... scattering on boundaries

τ_D ... point defect scattering

τ_u ... "Umklapp" processes

τ_E ... scattering on electrons

C is a constant and θ_D is the Debye temperature

The measured thermal conductivity (λ), the lattice contribution (λ_{ph}), the Callaway fit and the electronic part (λ_e) are shown in figure 8 for $Ba_8Au_6Ge_{40,}$ in figure 9 for $Ba_8Au_{5.1}Si_{40.9}$ and in figure 10 for $Ba_8Ag_5Si_{41.}$

The used user defined functions and explanations of the fitting parameter are taken from [8]. All parameter from the Callaway fit are summed in table 2.

References

[1] H.Anno, M. Hokazono, H. Takakura, K. Matsubara *ICT* (2005)

[2] N. Jaussaud, P. Gravereau, S. Pechev, B. Chevalier, M. Menetrier, P. Dordor, R. Decourt, G. Goglio, C. Cros, M. Pouchard *C.R.Chimie* **8** (2005) 39-46

[3] Rüdiger F.W. Herrmann, Katsumi Tanigaki, Sadanori Kuroshima, Hiroyoshi Suematsu *Chemical Physics Letters* **283** (1998) 29-32

[4] S. Johnsen, B. Thomsen, M. Christensen, G.K.H. Madsen, M. Nygren and B. Iversen *ICT* 2007

[5] Stefan Berger *Novel thermoelectric materials,* PhD thesis, TU Vienna (2003)

[6] J.H. Chiu *Phys. Review B* **13** (1976) 1507

[7] Callaway J and Baeyer H C 1960 *Phys. Rev.* **120** 1149

[8] Ingeborg Bednar *Diploma Thesis*: Thermoelectric properties of novel clathrates $Ba_8T_xT'_yGe_{46-x-y}$ (T = Cu,Si,Pd; T' = Zn) and $Ba_8Ag_zGe_{46-z}$ (z = 2,3,4,5) (2009)

Tables

Table 1: fit parameter for the Bloch-Grüneisen and the 2-band model with Mott-Jones term

fit para.	#A	#B	#C	#D	#E	#F	#G	#H
Bloch - Grüneisen	ρ_0 [$\mu\Omega$cm]	***R*** [$\mu\Omega$cm/K]	θ_D [K]	-	-	-	-	-
2-band model (Mott-Jones)	***R*** [$\mu\Omega$cm/K]	E_g [K]	n_0	$N(E)$ [1/J]	ρ_0 [$\mu\Omega$cm]	θ_D [K]	$(E-E_F)$ [K]	prefact
$Ba_8Ag_5Si_{41}$	750,3	321	474,9	-	-	-	-	-
	345,6	19620	1,112	4,073e+11	748,4	446,2	0,49	1e-9
$Ba_8Au_5Si_{41}$	1080,3	5324,5	0,915	1,02e+21	2970	730,1	9,98e-3	1e-6
$Ba_8Au_6Ge_{40}$	100.00	3276.4	0.6212	5.28e+19	478.7	156.8	7,23e-3	2.4e-12

R ... electron-phonon interaction constant [$\mu\Omega$cm/K]

E_g ... energy gap [K]

n_0 ... residual charge carrier density

$N(E)$ ... density of state [1/J]

ρ_0 ... residual resistivity [$\mu\Omega$cm]

θ_D ... Debye temperature [K]

$(E-E_F)$ ... energy difference between the Fermi energy and the lower band edge [K]

Table 2: fit parameter Callaway-model

fit parameter	#A	#B	#C	#D	#E	#F
Callaway-model			τ_B^{-1}		θ_D	
$Ba_8Au_6Ge_{40}$	3138.93	0.05765	95332526	7108682.4	300.59	$9.13066 \cdot 10^{-7}$
$Ba_8Au_5Si_{40}$	2444.49	21842.25	70220397	1714800.8	199.00	$1.20983 \cdot 10^{-6}$
$Ba_8Ag_5Si_{41}$	0.07185	17531.26	$7.54214 \cdot 10^8$	8273046.3	30.57	$1.76896 \cdot 10^{-6}$

F1 = #A *\$^4*X^4 … τ_D^{-1}

F2 = #B*\$^2*X^3*EXP(-#E/(3*X)) ... τ_U^{-1}

F3 = #C ... τ_B^{-1}

F4 = #D*X*\$ ... τ_E^{-1}

\$ … dummy variable of integration

#A … parameter for scattering processes on defects

#B … parameter for umklapp-processes

#C … boundary scattering

#D … parameter for scattering of phonons by electrons

#E … Debye temperature [K]

#F ... parameter of correction of radiation loss

Figures
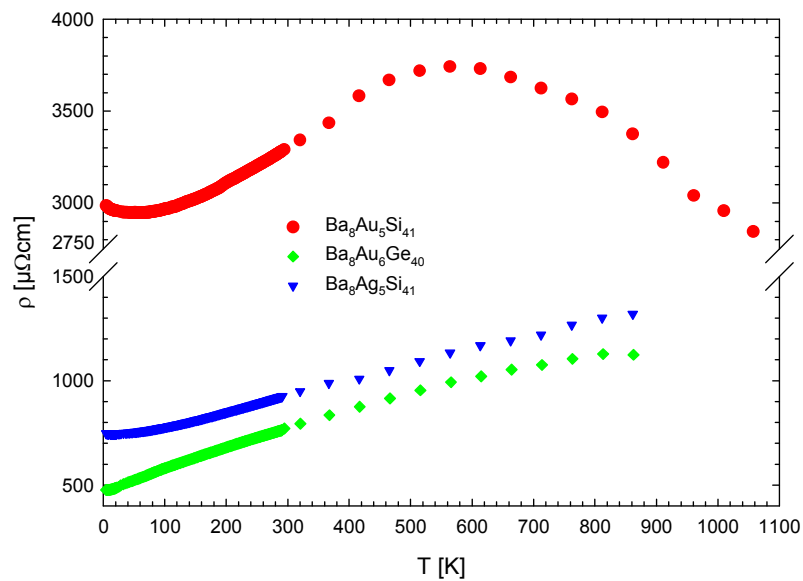
Fig. 1: temperature dependency of the electrical conductivity for the samples $Ba_8Au_6Ge_{40}$, $Ba_8Ag_5Si_{41}$ and $Ba_8Au_5Si_{41}$

.
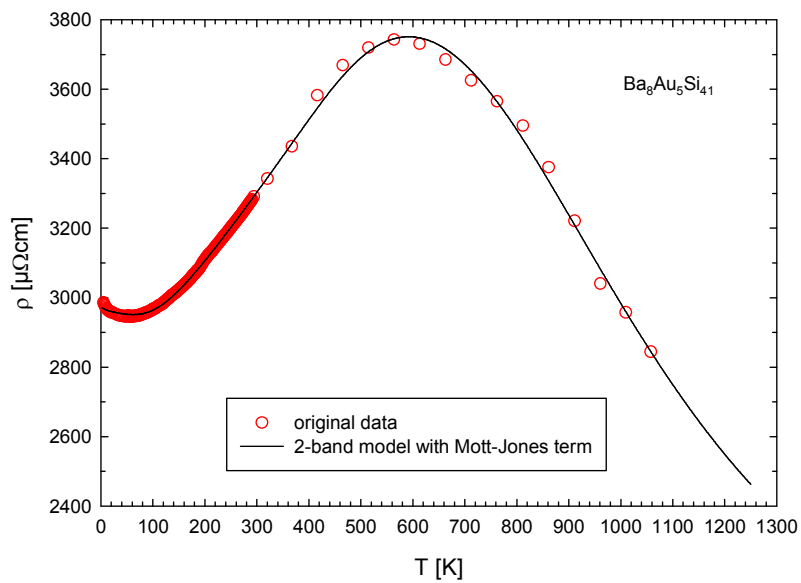
Fig. 2: temperature dependent electrical resistivity for $Ba_8Au_5Si_{41}$
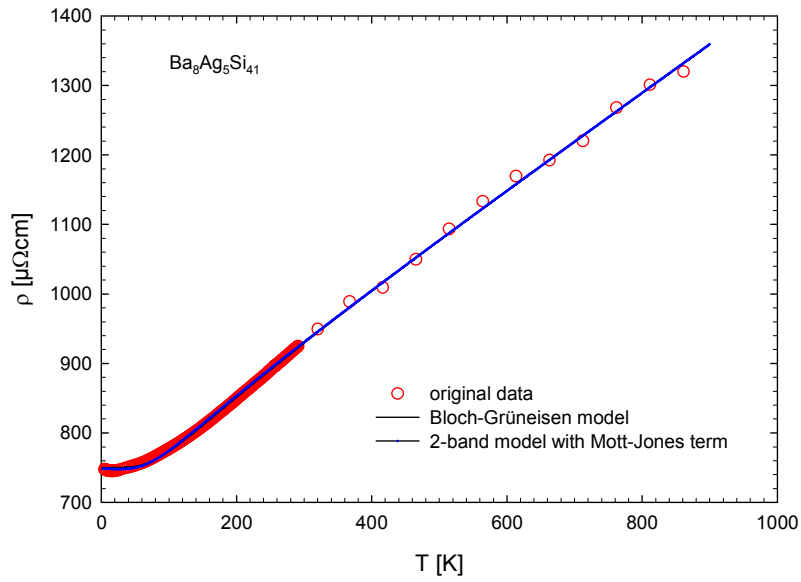
Fig. 3: temperature dependent electrical resistivity for $Ba_8Ag_5Si_{41}$
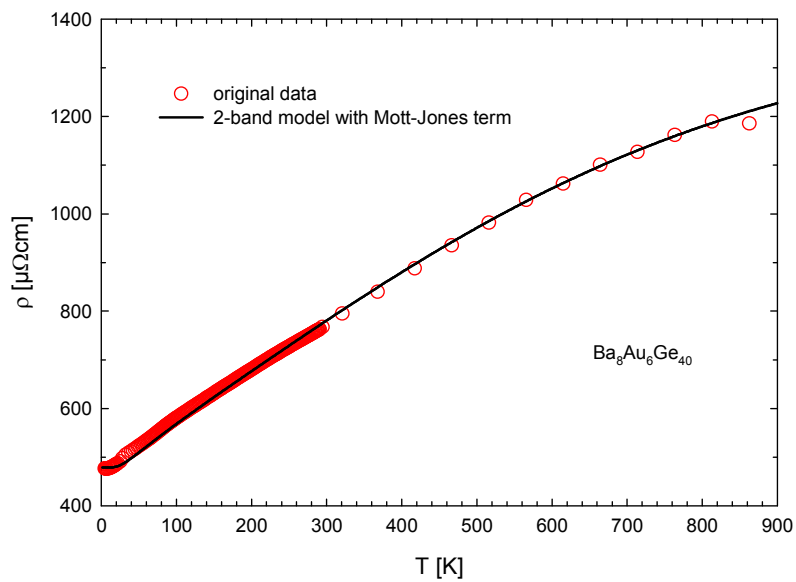
Fig. 4: temperature dependent electrical resistivity for $Ba_8Au_6Ge_{40}$
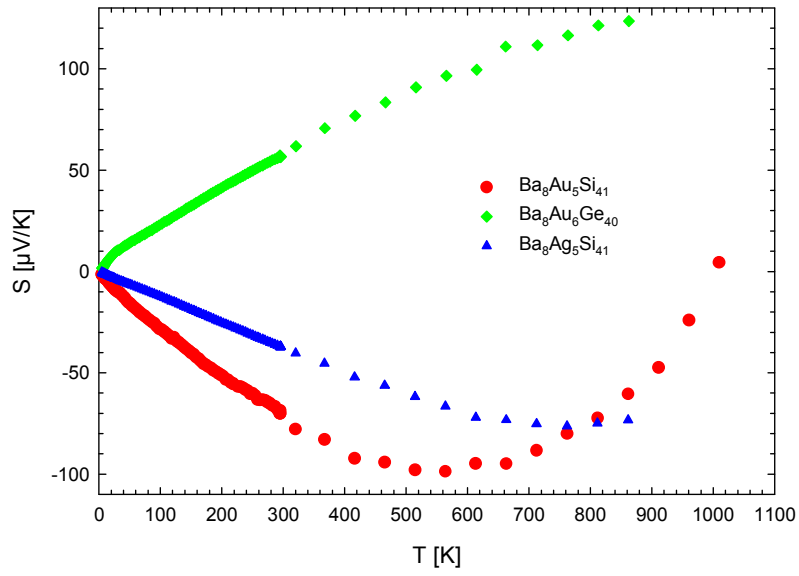
Fig. 6: temperature dependent thermopower S for $Ba_8Au_{5.1}Si_{40.8}$, $Ba_8Ag_5Si_{41}$ and $Ba_8Au_6Ge_{40}$
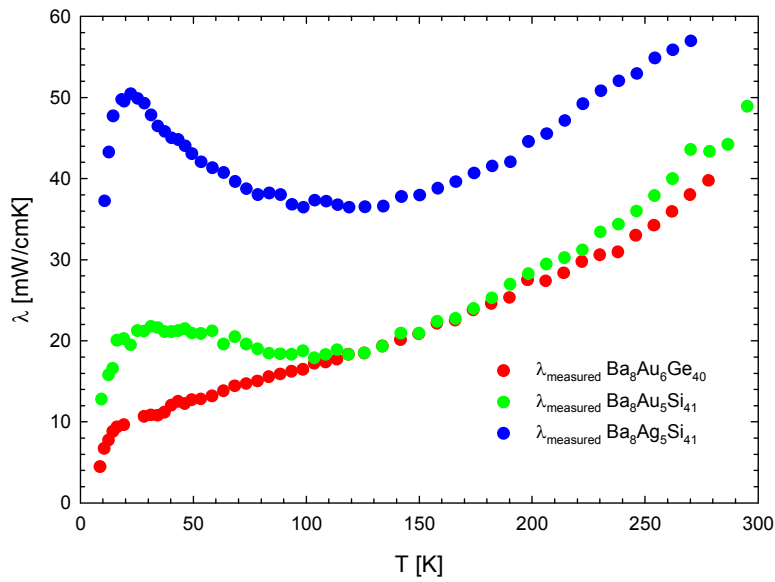
Fig. 7: temperature dependent thermal conductivity $\lambda(T)$ below 300K
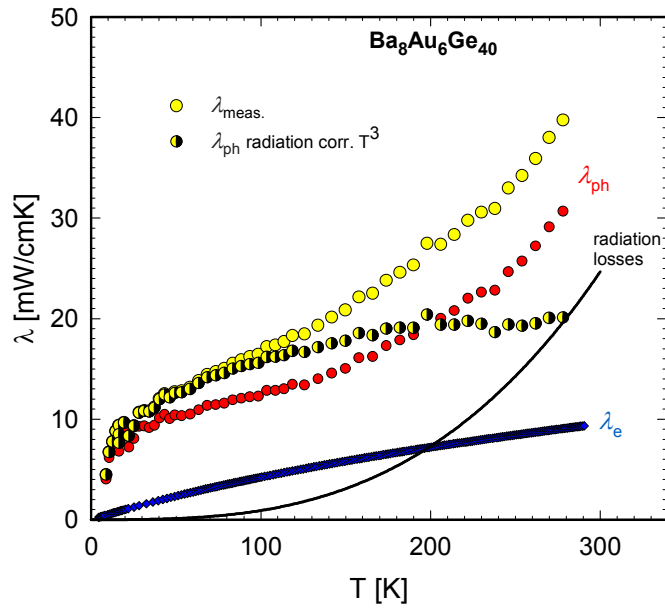
fig. 8: measured thermal conductivity (λ), the lattice contribution (λ_{ph}) , the electronic part (λ_e) and the radiation loss corrected lattice thermal conductivity for $Ba_8Au_6Ge_{40}$
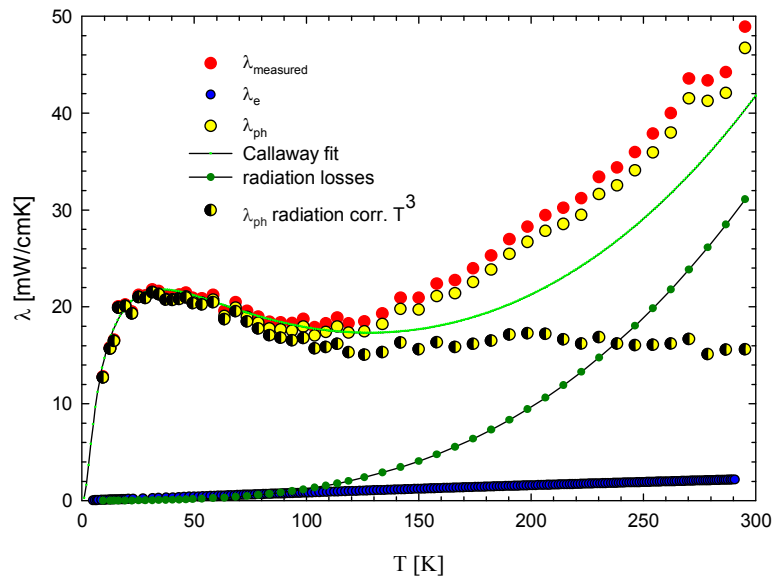
fig. 9: measured thermal conductivity (λ), the lattice contribution (λ_{ph}) , the Callaway fit, the electronic part (λ_e) and the radiation loss corrected lattice thermal conductivity for $Ba_8Au_{5.1}Si_{40.9}$
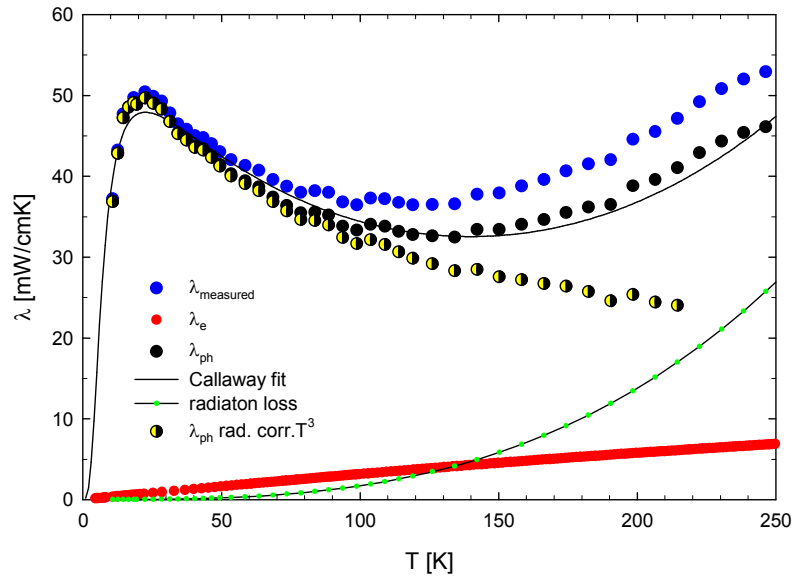
Fig. 10: measured thermal conductivity (λ), the lattice contribution (λ_{ph}) , the Callaway fit, the electronic part (λ_e) and the radiation loss corrected lattice thermal conductivity for $Ba_8Ag_5Si_{41}$

Acknowledgement

Curriculum Vitae

NAME: Isolde Zeiringer

Date of Birth: 21.02.1983

Nationality: Austria

Career Structure

2001- 2010   Chemistry studies in Vienna, focus on material science

1993 – 2001   Grammar School BRG St. Veit/ Glan, A levels

1989 – 2001   Primary School